

Summer School on Cosmology | (SMR 3945)

17 Jun 2024 - 28 Jun 2024
ICTP, Trieste, Italy

P01 - ADAMO Joseph Dominick

Neural network based emulation of galaxy power spectrum covariances - A re-analysis of BOSS DR12 data

P02 - ALVES MOURA José Roberto

Updated Big Bang Nucleosynthesis Bounds on Long-lived Particles from Dark Sectors

P03 - BELARBI Oussama Abdelghafour

On topological observables in 4D (gauge-affine) gravity and their possible cosmological implications.

P04 - BHARGAVA Parth

Stochastic Dynamics during Inflation

P05 - BOCHNAK Magdalena Marzena

Dark matter perturbations in LeDM model and their impact on cosmological tensions.

P06 - BURKMAR Molly Louise

Non-Singular Cosmology from Non-Linear Dark Energy

P07 - BUTSARACOM Kritaporn

Explanations of AMS-02 Electron and Positron Spectrum by Pulsar Wind Nebulae and Dark Matter Annihilation

P08 - CASAS DEL POZO Laura

Mock Universes via CoLoRe and LyaCoLoRe

P09 - CHIARENZA Sofia

Fast and accurate computation of 3x2pt statistics for weak lensing surveys

P10 - COLANGELI Elena

"Testing Modified Gravity Using Multimessenger Gravitational Wave Events"

P11 - COLOMA NADAL Jose María

Halo Bias and the Hierarchical Cosmic Web

P12 - COSTANTINI Andrea

Numerical methods for inflationary correlators.

P13 - CROSS Dane Noelle

Inverse Galaxy-Galaxy Lensing: Magnification, Intrinsic Alignments, and Cosmology

P14 - DAEI RASOULI Arefeh

Investigating the Homogeneity and Isotropy of the Universe with Large-scale Structure Data and the Consistency of our Motion to CMB

P15 - DUBE Yolanda

Detecting the power spectrum turnover with SKAO & other surveys

P16 - ESTRADA LLESTA Alejandro

Numerical construction of non linear initial data sets for cosmological models

P17 - FIGUEROA HERNÁNDEZ Juan Diego

Binary Neutron Star Systems as Super-Emitters of Gravitational Waves

P18 - GAMBARELLA Giosuè

On the range of validity of perturbative models for galaxy clustering and its uncertainty.

P19 - GIRI Rupal Pramod

Correlation between the X-ray morphology and the presence of diffuse radio emission sources in galaxy clusters.

P20 - GOMEZ AGUILAR Tadeo Dariney

Constraints on primordial black holes for nonstandard cosmologies

P21 - HOLLAND Hugo Alex Edouard

The separate universe approach in multifield inflation models

P22 - INGRAO Roberto

Projection Bias in Optically Selected Galaxy Clusters for Euclid Survey

P23 - KHOMERIKI Giorgi

Mixing Bispectrum Multipoles Under Geometric Distortions

P24 - LAHIRI Adhishree

Investigating the Galaxy Cluster A3407 and the Surrounding Large-Scale Structure using eROSITA Data

P25 - NAGAINIS Kristers

Emulator for three-point correlation function

P26 - NAIDOO Noeleen

Analysis of the boundary condition and equation of state in radiating stars

P27 - NAMDAR Mohammadhossein

Monge-Ampere Gravity at Cosmological Scales

P28 - NANDA Ayan

Self-Similarity of Halo Shapes for Power-law EdS Universe

P29 - PANDYA Aditya Jitendra

Examining cosmic (an)isotropy using velocity dispersion scaling relations of galaxy clusters

P30 - RANJBAR Maryamalsadat

Gravitational Slip Parameter and Gravitational Waves in Einstein-Cartan theory

P31 - DIAS RODRIGUES Daniel

Modelling the stellar neutrino spectrum

P32 - SAMARIO NAVA Sofía Del Pilar

Covariance matrices for 3-point correlation functions in photometric galaxy surveys.

P33 - SEKATCHEV Michael Igor

Axion Quark Nugget Annihilation Versus Observed Excess in Galactic Emissions

P34 - SEN Siddhant

Self similar collapse of a tri-axial halo with baryons in an EdS Universe

P35 - SHAH Neel Atul

Constraining Horndeski Gravity on Cosmological Scales

P36 - SURESHKUMAR Unnikrishnan Potty

Exploring the correlations between galaxy properties and environment in the cosmic web using marked statistics

P37 - THUMMEL Linus

Testing Beyond- Λ CDM Cosmologies with Neural Networks

P38 - TORABI GHADIM Nooshin

Detectability of PBHs by Lensed GW events

P39 - VALLIN SIMAO Bruna

Effects of Dark Matter Particles in Compact Objects and Observational Constraints

P40 - VICENTE João Gabriel

A line-of-sight CMB integrator for nearly-isotropic Bianchi models

P41 - WINKLER Lukas

Cosmological Field-Level Inference using Fast Differentiable Integrators

P42 - YANG Chen

Boundary Correlators with Strongly-Coupled Exchange

P43 - ZENTENO GATICA Cristóbal Tomas

Multifield inflation with massive fields and its impacts on early universe cosmological observables.

Neural network based emulation of galaxy power spectrum covariances - A re-analysis of BOSS DR12 data

J. Adamo¹, H.J. Huang¹, and T. Eifler¹

¹(*Presenting author underlined*) *Department of Astronomy/Steward Observatory, University of Arizona*

Typical methods of generating covariance matrices for use in a cosmological analysis require specifying an input cosmology. This dependence can be addressed by sequentially updating an assumed fiducial cosmology, or by varying covariance along with the model vector during an MCMC analysis. Previous work has shown the choice of method can affect the resulting parameter constraints [2, 3, 4], however such studies are commonly hampered by the computational cost of recalculating covariance at each new cosmology.

We present a neural network emulator that can quickly generate large-scale structure power spectrum covariance matrices from a given parameter set. This emulator utilizes a combination of traditional network layers and transformer architecture to generate redshift-space galaxy power spectrum multipole covariance matrices for the high redshift, north galactic cap sample of the BOSS DR12 galaxy catalog [1, 6]. We quantify performance by running simulated likelihood analyses varying the covariance matrix with cosmology. The resulting contours produced by our emulator have best fit values that agree to within 0.15σ , and error bars to within 4.6%, when comparing to chains run with analytic covariance calculations. Similar results are achieved when varying the Gaussian covariance, suggesting our network is robust to different model configurations.

We end by using our emulator to perform a re-analysis of the BOSS power spectrum with the same configuration as Ref. [5]. We find that varying covariance with cosmology along with the model vector introduces an average 0.46σ shift in best-fit values and a 5% increase in constraining power. This result suggests that cosmology-dependent covariance can matter for full-shape power spectrum analyses, and should be considered for upcoming spectroscopic surveys like from the Dark Energy Spectroscopic Instrument (DESI) and the SPHEREx mission.

- [1] F. Beutler, P. McDonald, JCAP. **2021**, 031 (2021).
- [2] T. Eifler, P. Schneider, J. Hartlap, AAP. **502**, 721 (2009).
- [3] Fumagalli et al. (Euclid Collaboration), arXiv e-print. **arXiv:2211.12965** (2022).
- [4] A. Labatie, J. L. Starck, M. Lachi'eze-Rey, ApJ. **760**, 97 (2012).
- [5] D. Wadekar, M. M. Ivanov, R. Scoccimarro, Phys. Rev. D. **102**, 123521 (2020).
- [6] D. Wadekar, R. Scoccimarro, Phys. Rev. D. **102**, 123517 (2020).

Updated Big Bang Nucleosynthesis Bounds on Long-lived Particles from Dark Sectors

J. R. Alves^{1,2}, L. Angel^{1,2}, R. M. P. Neves², F. S. Queiroz^{1,2,3}, D. R. da Silva^{2,5}, R. Silva¹, and Y. Villamizar⁶

¹*(Presenting author underlined) Affiliation 1*

²*Affiliation 2*

As electromagnetic showers may alter the abundance of Helium, Lithium, and Deuterium, we can place severe constraints on the lifetime and amount of energy injected by long-lived particles decaying into dark matter. Considering up-to-date measurements of the light element abundances that point to $Y_p = 0.245 \pm 0.003$, $(D/H) = (2.527 \pm 0.03) \times 10^{-5}$, $({}^7\text{Li}/H) = 1.58_{-0.28}^{+0.35} \times 10^{-10}$, $({}^6\text{Li}/{}^7\text{Li}) = 0.05$, and the baryon-to-photon ratio obtained from the Cosmic Microwave Background data, $\eta = 6.14 \times 10^{-10}$, we derive upper limits on the fraction of electromagnetic energy produced by long-lived particles. Our findings are applicable to decaying dark matter models, and non-thermal processes that occurred in the early universe between 10^2 and 10^{10} seconds.

- [1] Alves, J., Angel, L., Guedes, L., Neves, R., Queiroz, F., Silva, D., Silva, R. & Villamizar, Y. Updated Big Bang Nucleosynthesis Bounds on Long-lived Particles from Dark Sectors. (2023)

On topological observables in 4D (gauge-affine) gravity and their possible cosmological implications

Oussama A. Belarbi¹ and Ahmed Meziane¹

¹*Laboratoire de Physique Théorique d'Oran (LPTO), Université Oran 1 Ahmed Ben Bella, B.P 1524 El M'Naouer, Oran 31000*

We provide a general outline on the calculation of observables for 4D topological (gauge) theories of gravity, e.g. topological gravity and topological gauge-affine gravity [1], using the BRST superspace approach [2]. The emphasis is on the latter with an outlook on the possibility of constructing further observables in the same 4D topological model. Then, inspired by relatively recent works [3, 4, 5], we give possible implications of such observables in cosmology, namely in early stage of the universe and in inflation models.

- [1] O. A. Belarbi, A. Meziane, To appear in *Symmetry*, MDPI (2024).
- [2] O. A. Belarbi, A. Meziane, *AIP Conf. Proc.* **2872**, 060005 (2023).
- [3] S. Lazzarini, J. Thibaut, arXiv preprint arXiv:2403.05284 [gr-qc] (2024).
- [4] P. Agrawal, S. Gukov, G. Obied, C. Vafa, arXiv preprint arXiv:2009.10077 [hep-th] (2020).
- [5] G. Pollari, arXiv preprint arXiv:2308.03145 [gr-qc] (2023).

Stochastic Dynamics during Inflation

Parth Bhargava¹, Hooshyar Assadullahi^{1,2}, Kazuya Koyama¹, and David Wands¹

¹*Institute of Cosmology & Gravitation, University of Portsmouth, Dennis Sciama Building, Burnaby Road, Portsmouth, PO1 3FX, United Kingdom*

²*School of Mathematics and Physics, University of Portsmouth, Lion Gate Building, Lion Terrace, Portsmouth, PO1 3HF, United Kingdom*

The classical evolution of fields during a period of rapid accelerated expansion in the very early universe (“inflation”) can establish an idealised homogeneous and isotropic cosmology, but quantum fluctuations inevitably generate inhomogeneities and anisotropies on all observable scales (and beyond). In the stochastic approach to modeling inflationary dynamics [1], these quantum field fluctuations are incorporated as stochastic noise. We use the formalism of stochastic inflation to investigate the role of quantum diffusion during inflation in the very early universe. Quantum fluctuations in the duration of inflation lead to primordial density perturbations after inflation [2]. This provides a non-perturbative framework to study cosmological fluctuations during inflation, which is well-suited to the case of primordial black holes since they originate from large fluctuations [3, 4]. We use the numerical code PyFPT [5] to explore the occurrence of rare, very large fluctuations in slow-roll inflation models which may have a highly non-Gaussian distribution.

- [1] A. A. Starobinsky, “STOCHASTIC DE SITTER (INFLATIONARY) STAGE IN THE EARLY UNIVERSE,” *Lect. Notes Phys.* **246** (1986), 107-126
- [2] V. Vennin and A. A. Starobinsky, “Correlation Functions in Stochastic Inflation,” *Eur. Phys. J. C* **75** (2015), 413 [arXiv:1506.04732 [hep-th]].
- [3] C. Pattison, V. Vennin, H. Assadullahi and D. Wands, “Quantum diffusion during inflation and primordial black holes,” *JCAP* **10** (2017), 046 [arXiv:1707.00537 [hep-th]].
- [4] J. M. Ezquiaga, J. García-Bellido and V. Vennin, “The exponential tail of inflationary fluctuations: consequences for primordial black holes,” *JCAP* **03** (2020), 029 [arXiv:1912.05399 [astro-ph.CO]].
- [5] J. H. P. Jackson, H. Assadullahi, K. Koyama, V. Vennin and D. Wands, “Numerical simulations of stochastic inflation using importance sampling,” *JCAP* **10** (2022), 067 [arXiv:2206.11234 [astro-ph.CO]].

Dark matter perturbations in an evolving DM (LeDM) model and their impact on cosmological tensions

Magdalena Bochnak¹, Mariana Jaber², Krishna Naidoo³

¹*Jagiellonian University, Krakow, Poland*

²*Center on Theoretical Physics PAS, Warsaw, Poland*

³*University College London, London, England*

In [1] the authors consider a phenomenological model of dark matter (DM) with an equation of state that is negative and changing at late times, which is called the LeDM model. The model introduced in that work couples the H_0 and σ_8 tensions, proposing a solution to both simultaneously, while also explaining the anomalously large integrated Sachs-Wolfe (ISW) effect from cosmic voids.

As a working hypothesis, the authors of [1] assume a null speed of sound for the perturbations of the eDM component. In this work, we explore the consequences of removing that assumption and investigate the effect on the growth of perturbations. By rederiving and solving the equations for the evolution of density contrast in the Newtonian approach, we analyse the impact of a time-changing equation of state in the speed of sound of dark matter perturbations and its solutions as a function of time. We compare our solutions against the standard Einstein de-Sitter (EdS) and dust solutions (a cold pressureless dark matter component).

The LeDM model presents an equation for DM with two free parameters: the present-day value of the equation of state, w_0 , and a transition epoch. Our preliminary results show that for some values of these free parameters, in particular the value of w_0 , the solutions to the evolution of density contrast will have an oscillatory behaviour, and for other values, we shall have an unstable gravitational growth. Their impact is studied in the framework of the Jeans instability analysis. Finally, adding the resulting logarithmic growth function, $f=d\log D/d\log a$, for different values of the LeDM model, we can discuss the observational imprints of this model in the structure formation at large scales. These results will be presented in [2].

[1] Naidoo K., Jaber M., Hellwing W.A., Bilicki M., 2022, arXiv, arXiv:2209.08102.

doi:10.48550/arXiv.2209.08102 (accepted for publication in PRD)

[2] Magdalena Bochnak, “Dark matter perturbations in an evolving LeDM model and their impact on cosmological tensions” (work in progress to obtain the degree of Master in Science by the Jagiellonian University of Krakow)

Non-Singular Cosmology from Non-Linear Dark Energy

ICTP Summer School on Cosmology

Molly Burkmar¹ and Marco Bruni^{1,2}

¹Institute of Cosmology & Gravitation, University of Portsmouth, Dennis Sciama Building, Burnaby Road, Portsmouth, PO1 3FX, United Kingdom

²INFN Sezione di Trieste, Via Valerio 2, 34127 Trieste, Italy

The Standard Model of Cosmology provides a successful framework for the history of our Universe, however there are problems which require addressing. A key problem is that singularities arise at high energies, and their current interpretation is that they represent points where General Relativity (GR) breaks down. Therefore, it is worth considering an alternative to the 'Big Bang' as the origin story of the Universe. Bouncing and emergent cosmologies provide a way to evade this singularity, and can be produced by a dynamic dark energy within GR [1]. To ensure this scenario can be realistic, dark matter and radiation need to be included in the set-up to understand whether the non-singular behaviour is still possible. In this talk, I will first present the dynamics of non-singular models produced by a dark energy which evolves between two cosmological constants, showing the effect of including non-interacting dark matter and radiation, and explain the caveats to these models [2]. I will then present the dynamics when a non-gravitational interaction term is included between the dark components. Interestingly, I will show that there are emerging models that are past asymptotic to a de Sitter fixed point, which differs from other emergent models in GR where the past attractor is an Einstein state [3].

References

- [1] Kishore N. Ananda and Marco Bruni. Cosmological dynamics and dark energy with a nonlinear equation of state: A quadratic model. *Phys. Rev. D*, 74:023523, 2006.
- [2] Molly Burkmar and Marco Bruni. Bouncing cosmology from nonlinear dark energy with two cosmological constants. *Phys. Rev. D*, 107:083533, 4 2023.
- [3] George F R Ellis and Roy Maartens. The emergent universe: Inflationary cosmology with no singularity. *Class. Quant. Grav.*, 21:223–232, 2003.

Explanations of AMS-02 Electron and Positron Spectrum by Pulsar Wind Nebulae and Dark Matter Annihilation

Kritaporn Butsaracom^{1,2}, Brandon Khan Cantlay^{1,2}, and Maneenate Wechakama^{1,2}

¹*Department of Physics, Faculty of science, Kasetsart University, Bangkok, 10900, Thailand*

²*National Astronomical Research Institute of Thailand (Public Organization), Chiangmai, 50180, Thailand*

We aim to study the latest data of the Alpha Magnetic Spectrometer-02 (AMS-02) electron plus positron spectrum (2021) [1]. This spectrum provides data in the energy range from 0.5 GeV to 1664.5 GeV, updated from 2019. In this research, we investigate the excess of electrons and positrons by comparing it with the background spectrum derived from a broken power law [2]. We focus on the electron plus positron spectrum above 10 GeV. The electron and positron spectrum at low energy is dominated by Solar modulation. We employ the pulsar wind nebulae (PWNe) [3] and dark matter annihilation [4] models to explain the excess of electrons and positrons. We assume that electrons and positrons can propagate into space up to 1 kpc. We utilize specific data from the Australia Telescope National Facility (ATNF) pulsar catalogue [5]. For the PWN model, we examine the electron and positron spectrum from a single PWN and multiple PWNe models. Utilizing multiple PWNe models improves the interpretation of the excess of electrons and positrons. Finally, we contribute the electron and positron spectrum from the single PWN and dark matter annihilation model in each channel, which enhances the explanation of the excess of electrons and positrons.

- [1] Aguilar, M., Cavasonza, L. A., Ambrosi, G., Arruda, L., Attig, N., Barao, F., ... Pashnin, A., *Physics reports* **894**, 1-116 (2021).
- [2] Zu, L., Zhang, C., Feng, L., Yuan, Q., Fan, Y. Z. *Physical Review D*, **98(6)**, 063010. (2018).
- [3] Ding, Y. C., Li, N., Wei, C. C., Wu, Y. L., Zhou, Y. F. *Physical Review D*, **103(11)**, 115010. (2021).
- [4] Wechakama, M., Ascasibar, Y. *Monthly Notices of the Royal Astronomical Society*, **439(1)**, 566-587. (2014).
- [5] Coles, W. A., Kerr, M., Shannon, R. M., Hobbs, G. B., Manchester, R. N., You, X. P., ... Zhu, X. J. *The Astrophysical Journal*, **808(2)**, 113. (2015).

Mock Universes via CoLoRe and LyaCoLoRe

Laura Casas

¹Institut de Física d'Altes Energies. The Barcelona Institute of Science and Technology, Campus UAB, 08193 Bellaterra (Barcelona), Spain

Lyman alpha forests are a recent and promising area of research which opens cosmology to the high redshift universe. Using Lyman Alpha absorption we are able to build 3D maps of matter distribution which can be used to study the structure of the universe at large scales. In this context, the utilization of mock datasets becomes important for the accurate interpretation of measurements, correlation analysis, and systematic error correction. Within the DESI Lyman alpha group we have used CoLoRe[1] and LyaCoLoRe[2] to create mocks. They are public software packages that generate realisations of cosmological surveys which have been very useful in eBoss DR16 and in DESI Y1 analyses. In this presentation I will give an overview of how mocks are done within the Lyman alpha forest group in DESI, focusing in CoLoRe and LyaCoLoRe and explain ways we are trying to improve them.

[1] C. Ramírez-Pérez, J. Sanchez, D. Alonso, A. Font-Ribera, *CoLoRe: fast cosmological realisations over large volumes with multiple tracers*. JCAP 05 (2022) 05, 002 [[2111.05069](#)].

[2] J. Farr, A. Font-Ribera, H. du Mas des Bourboux, A. Muñoz-Gutiérrez, F. J. Sánchez, A. Pontzen et al., *LyaCoLoRe: synthetic datasets for current and future Lyman- α forest BAO surveys*, J. Cosmology Astropart. Phys. 2020 (2020) 068 [[1912.02763](#)].

Fast and accurate computation of 3x2pt statistics for weak lensing surveys

March 29, 2024

Abstract

The accurate computation of 3x2pt statistics plays a crucial role in understanding the large-scale structures in the universe using cosmological surveys. While the Limber approximation has traditionally provided a simple and efficient method for this computation, its limitations become apparent in the context of recent and future surveys, demanding more precise and efficient techniques. In this work, we propose a novel, computationally fast, approach to compute 3x2pt statistics without relying on the Limber approximation, ensuring both efficiency and precision.

Our method addresses the challenge of dealing with a 3D integral with Bessel functions by employing a combination of techniques, effectively handling the oscillatory nature of the Bessel functions.

An important aspect of our approach is its compatibility with automatic differentiation techniques, facilitating likelihood exploration and maximization even in high-dimensional parameter space. This feature enhances the usability of our method in cosmological parameter estimation tasks.

Overall, our proposed method offers a promising solution for accurately computing 3x2pt statistics in upcoming cosmological surveys, addressing the shortcomings of the Limber approximation and providing a valuable tool for extracting information from large-scale structure. In particular, the tool provided will be of critical importance for the Euclid survey, enabling the core scientific analyses to be performed using modern statistical inference techniques.

Testing Modified Gravity Using Multimessenger Gravitational Wave Events

Elena Colangeli¹, Tessa Baker¹, Konstantin Leyde¹

¹Institute of Cosmology & Gravitation, University of Portsmouth, Dennis Sciama Building, Portsmouth, PO1 3FX, UK

This study explores joint estimation of the Hubble constant and parameters describing Horndeski's theory of modified gravity through the analysis of gravitational wave (GW) multimessenger signals. Horndeski theory is the most general scalar-tensor theory that produces second-order field equations and it provides a promising framework for explaining effects such as the accelerated expansion of the universe [1]. The advent of gravitational wave astronomy offers new ways to test the predictions of modified gravity theories, in particular with the detection of the first event with an electromagnetic counterpart, GW170817 [2][3]. This work is a starting point to prepare for new data incoming with the latest LIGO observation runs. A toy model is considered in order to constrain Horndeski parameters and H_0 for multimessenger events, with plans to implement the method for dark sirens (GW events without electromagnetic counterparts) in the future.

[1] Horndeski GW. Second-order scalar-tensor field equations in a four-dimensional space. *International Journal of Theoretical Physics*. 1974 Sep;10:363-84.

[2] Abbott BP et al. GW170817: observation of gravitational waves from a binary neutron star inspiral. *Physical review letters*. 2017 Oct 16;119(16):161101.

[3] Lagos M, Fishbach M, Landry P, Holz DE. Standard sirens with a running Planck mass. *Physical Review D*. 2019 Apr 5;99(8):083504.

Halo Bias and the Hierarchical Cosmic Web

J. M. Coloma Nadal¹, F.-S. Kitaura^{2,3}, J. E. García-Farieta^{2,3}, F. Sinigaglia^{2,3,4,5}, G. Favole^{2,3} and D. Forero Sánchez⁶

¹*Institute of Space Sciences (ICE, CSIC), Campus UAB,
Carrer de Can Magrans, s/n, 08193 Barcelona, Spain*

²*Instituto de Astrofísica de Canarias,
Calle Via Láctea s/n, E-38205, La Laguna, Tenerife, Spain*

³*Departamento de Astrofísica, Universidad de La Laguna,
E-38206, La Laguna, Tenerife, Spain*

⁴*Département d'Astronomie, Université de Genève,
Chemin Pegasi 51, CH-1290 Versoix, Switzerland*

⁵*Institut für Astrophysik, Universität Zürich, Winterthurerstrasse 190, CH-8057 Zürich,
Switzerland*

⁶*Institute of Physics, Laboratory of Astrophysics, École Polytechnique Fédérale de Lausanne
(EPFL), Observatoire de Sauverny, CH-1290 Versoix, Switzerland*

Accurate modeling of galaxy distributions is paramount for cosmological analysis using galaxy redshift surveys. However, this endeavor is often hindered by the computational complexity of resolving the dark matter halos that host these galaxies. To address this challenge, we propose the development of effective assembly bias models down to small scales. In our approach, we introduce a hierarchical cosmic web classification system that indirectly captures up to third-order long- and short-range non-local bias terms. This classification system also enables us to maintain positive definite parametric bias expansions. Specifically, we subdivide the traditional cosmic web classification, which is based on the eigenvalues of the tidal field tensor derived, with an additional classification based on the Hessian matrix of the negative density contrast. To assess the effectiveness of our model, we conducted tests using a halo catalog extracted from the UNITSIM simulation, which was run within a cubic box measuring $1 h^{-1}$ Gpc on each side. We obtained the large-scale dark matter cosmic web by evolving the corresponding initial conditions using a mesh comprised of 256^3 cells, employing Augmented Lagrangian Perturbation Theory. The resulting halo catalogs, generated through our approach, exhibit a high level of accuracy in terms of the two- and three-point statistics. They reproduce the reference power spectrum within better than 2% percent accuracy up to wavenumbers of approximately $k \sim 0.8 h \text{ Mpc}^{-1}$ and provide accurate bispectra within the scales that are crucial for cosmological analysis. This effective bias model holds significant potential for facilitating cosmological analysis using galaxy redshift surveys, particularly in the context of projects such as DESI, EUCLID, and LSST.

Numerical methods for Inflationary Correlators

Costantini A.¹, and Mulryne D.¹

¹(*Presenting author underlined*) *Queen Mary University of London*

In the inflationary scenario, quantum-mechanical processes seeded an initial distribution of gravitational wells that lead to cosmological structure formation in the late universe[1]. The analysis of the later time matter distribution can be used to infer details of the seeding process, and the quantities used in the analysis are the correlation functions describing the primordial distribution of the curvature perturbation ζ . The calculation of the correlation functions requires knowledge of quantum field theory in curved space-time and it is usually described as the In-In formalism applied to inflationary cosmology. Such calculations present several challenges difficult to overcome: the algebraic complexity arising when even the simplest models are coupled to gravity; and second, the occurrence of large hierarchies. The simplest solution is to switch to a numerical method.

A powerful method to calculate the correlation functions is the *transport approach* [2], which provides evolution equations for the two- and three-point correlation functions at least at the tree level. Since this method relies on differential equations, it is easy to implement numerically. Moreover, one can introduce objects, closely related to the correlations themselves, which allow formal analytic solutions of the transport hierarchy. These objects are the *van Vleck* or Γ matrices [2, 3] which are the propagators of the system, and allows to compute the correlations from some initial time t_0 to some later time t . They also obey to transport equations and so their evolution can be easily computed numerically.

PyTransport [4] is a package written in C++ and Python that employs the transport approach to inflationary cosmology to calculate the tree-level power-spectrum and bispectrum of multi-field inflation models. Our project consists of extending the PyTransport package in order to reproduce the results obtained with the 'standard' transport approach by using the Γ matrices instead. In the future, we will use these matrices to go beyond the tree level and include in our computation at least the one-loop corrections to the correlation functions.

- [1] M. Dias, J. Frazer, D. J. Mulryne and D. Seery, JCAP **12** (2016), 033 doi:10.1088/1475-7516/2016/12/033 [arXiv:1609.00379 [astro-ph.CO]].
- [2] D. J. Mulryne, JCAP **09** (2013), 010 doi:10.1088/1475-7516/2013/09/010 [arXiv:1302.3842 [astro-ph.CO]].
- [3] D. Seery, D. J. Mulryne, J. Frazer and R. H. Ribeiro, JCAP **09** (2012), 010 doi:10.1088/1475-7516/2012/09/010 [arXiv:1203.2635 [astro-ph.CO]].
- [4] D. J. Mulryne and J. W. Ronayne, J. Open Source Softw. **3** (2018) no.23, 494 doi:10.21105/joss.00494 [arXiv:1609.00381 [astro-ph.CO]].

Inverse Galaxy-Galaxy Lensing: Magnification, Intrinsic Alignments, and Cosmology

AUTHORS

Dane Cross
Carles Sánchez

AFFILIATIONS

Institut de Física d'Altes Energies (IFAE), The Barcelona Institute of Science and Technology, Campus UAB, 08195 Bellaterra (Barcelona), Spain
 Departament de Física, Universitat Autònoma de Barcelona (UAB), 08195 Bellaterra (Barcelona), Spain

Financial support from the 2019 Ramón y Cajal program RYC2019-027685-I and the PIE project 2021SA1016. This publication and other results have the support of the predoctoral program AGAUR Joan Orió of the Secretariat of Universities and Research of the Department of Research and Universities of the Generalitat of Catalonia and the European Social Plus Fund (2023 FL-1-00685).

IGGL PROBES THE INTERMEDIATE MASS DISTRIBUTION

Traditional Galaxy-Galaxy Lensing



Correlates the shape measurements with the positions of the lenses. Shapes at a smaller angular separation from the lens have a stronger lensing signal.

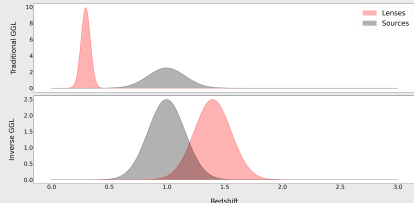
Inverse Galaxy-Galaxy Lensing



IGGL probes the effect of the intermediate mass distribution on source shapes + lens positions. Lens positions are no longer the "center" of the matter doing the lensing. So, this approach probes cosmology from the intermediate mass distribution.

INVERSE GALAXY GALAXY LENSING (IGGL)

As telescopes such as the Vera Rubin Observatory's Legacy Survey of Space and Time (LSST) obtain images of galaxies at higher and higher redshifts, we will have more data than ever to conduct weak lensing surveys. The traditional lensing paradigm has lens galaxies (galaxy positions) in front of source galaxies (galaxies with shape measurements). Source shapes require higher signal-to-noise than lens positions, so there are many high-redshift galaxy positions that do not have shape-measured galaxies behind them, so traditional galaxy-galaxy lensing cannot be performed. In this project, we explore how we can use high-redshift lenses with low-redshift sources (inverse of the traditional setup) to constrain both cosmology and systematic effects in weak lensing surveys.



Measurements of weak lensing are done by correlating average ellipticities of source (shape-measured) galaxies with positions of lens galaxies.

$$\delta_g^{obs} = \delta_g^{int} + \delta_g^{mag} \quad e^{obs} = \gamma + e^{int}$$

$$\langle \delta_g^{obs} e^{obs} \rangle = \langle (\delta_g^{int} + 2(\alpha - 1)\kappa_l)(\gamma + e^{int}) \rangle = \langle \delta_g^{int} \gamma \rangle + 2(\alpha - 1)\langle \kappa_l \gamma \rangle + \langle \delta_g^{int} e^{int} \rangle + 2(\alpha - 1)\langle \kappa_l e^{int} \rangle$$

trad GGL
lens mag
IA
lens mag + IA

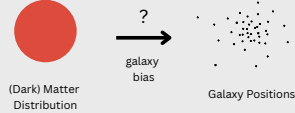
Switching lenses and sources removes the traditional GGL term, isolating the second order effects (2nd, 3rd, and 4th terms).

Tensions Between Measurements from the Early and Late Universe

- | | |
|--|--|
| <p>High redshift (early-universe):</p> <ul style="list-style-type: none"> CMB BAC <p>S₈ constraint:</p> <ul style="list-style-type: none"> 0.832 ± 0.013 ⁽¹⁾ <p>H₀ constraint:</p> <ul style="list-style-type: none"> (67.27 ± 0.6) km/(s Mpc) ⁽²⁾ | <p>Low redshift (late-universe):</p> <ul style="list-style-type: none"> Weak Lensing LSS Supernovae <p>S₈ constraint:</p> <ul style="list-style-type: none"> 0.840 ± 0.030 ⁽³⁾ <p>H₀ constraint:</p> <ul style="list-style-type: none"> (73.04 ± 1.04) km/(s Mpc) ⁽⁴⁾ |
|--|--|

These tensions could be caused by either incorrectly modeling second order effects or by new physics. One of the goals of this project is to explore an analysis that takes a closer look at these effects in an attempt to solve these tensions.

NO DEPENDENCE ON GALAXY BIAS ISOLATES BARYONIC EFFECTS



Galaxy bias and the effect of baryons at non-linear scales of the matter-power spectrum are virtually degenerate. IGGL removes galaxy bias dependence, allowing us to better examine baryonic effects on weak lensing at small scales.

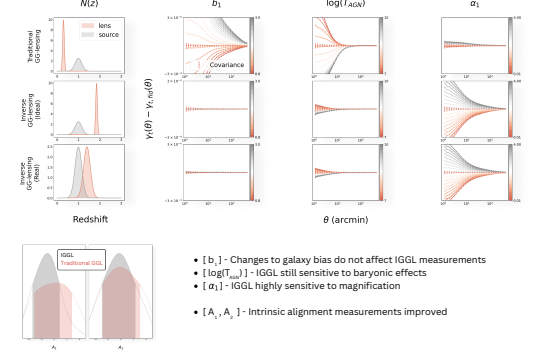
Since there is no galaxy bias, IGGL also doesn't require galaxy clustering measurements for cosmology results.

REFERENCES

1. L. Perivolaropoulos and F. Skara, "Challenges for ΛCDM: An update"
2. Planck Collaboration, N. Aghanim et al., "Planck 2018 results. VI. Cosmological parameters," *Astron. Astrophys.* 641 (2020)
3. A. G. Riess et al., "A Comprehensive Measurement of the Local Value of the Hubble Constant with 1 km/s/Mpc Uncertainty from the Hubble Space Telescope and the SH0ES Team (2020)"
4. Z. Zhang, C. Chang et al., "Transitioning from Stage-III to Stage-IV: Cosmology from galaxy×CMB lensing and shear×CMB lensing" (2022)
5. J. Prat et al., "Dark energy survey year 3 results: High-precision measurement and modeling of galaxy-galaxy lensing" (2022)

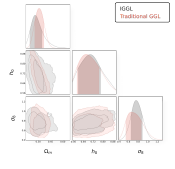
MODELLING WITH LSST PROJECTIONS

We use the cosmoSIS pipeline to make predictions for what we can constrain with IGGL. The choices for lens and source bin size and covariances are informed by projections from the Legacy Survey of Space and Time (LSST) Dark Energy Science Collaboration (DESC).



Cosmology

- Relative Signal-to-Noise Projections:
 - Traditional: 61.99
 - Inverse: 31.16
- Half the Signal-to-Noise still leads to better S₈ measurements
- No galaxy bias reliance improves S₈ measurement



Conclusions

- No impact of galaxy bias
 - No traditional GGL signal means no reliance on galaxy bias
 - No reliance on galaxy clustering to break bias degeneracy
- Isolation of baryonic effects
 - Galaxy bias and baryonic effects are difficult to separate, removal of galaxy bias dependence isolates baryonic effects
- Improved IA constraints
- Improved S₈ measurements with half the signal-to-noise

Investigating the Homogeneity and Isotropy of the Universe with Large-scale Structure Data and the Consistency of our Motion to CMB

Arefeh Rasouli¹, Shant Baghram¹, and Sohrab Rahvar¹

¹Department of Physics, Sharif University of Technology, Tehran 11155-9161, Iran

The standard Λ CDM model is built upon the cosmological principle, which states that the universe on large scales is homogeneous and isotropic when averaged over sufficiently large scales. However, the cosmic microwave background (CMB) displays a dipole anisotropy at a level of $\frac{\Delta T}{T} \sim 10^{-3}$. This dipole is commonly interpreted as owing to our motion with respect to the CMB rest frame. A model-independent approach to validate this kinematic hypothesis is to determine the dipole moment in the angular distribution of the large-scale structure at lower redshifts. Previous observations of the dipole anisotropy in the sky distribution of radio galaxies and quasars, drawn from NVSS and WISE catalogs, indicate a discrepancy with the CMB dipole, both in terms of direction and amplitude.[1, 2]

In this study, we investigate this inconsistency using large-scale cosmic data. Along with analyzing the Doppler effect, we will also explore the average peculiar velocity of structures and compare it with the standard model. In order to determine the true peculiar velocity, we are trying to distinguish between the kinematic and clustering dipoles. Additionally, we will look into new methods for measuring kinematic velocity and examine the impact of alternative models in resolving this discrepancy.

- [1] Nathan J. Secrest, Sebastian von Hausegger, Mohamed Rameez, Roya Mohayaee, Subir Sarkar, ApJ. **937**, L31 (2022).
- [2] Nathan J. Secrest, Sebastian von Hausegger, Mohamed Rameez, Roya Mohayaee, Subir Sarkar, Jacques Colin, ApJ. **908**, L51 (2021).

DETECTING THE POWER SPECTRUM TURNOVER WITH SKAO & OTHER SURVEYS

MSc Student: Yolanda Dube & Supervisor: Prof Roy Maartens

University of the Western Cape, Department of Physics & Astronomy

Power spectrum & turnover

- One of the main goals of cosmology is to understand the distribution of galaxies, galaxy clusters, and even larger cosmic structures like filaments and voids, i.e., the universe's large-scale structure.
- The power spectrum is a crucial observable in cosmology that encodes the large-scale structure of our universe.
- At ultra-large scales, the matter power spectrum exhibits a peak of interest known as the turnover, an essential probe for these scales.

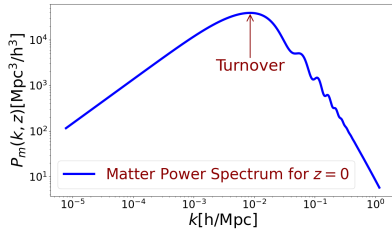


Figure 1: Shows the plot for the matter power spectrum for redshift $z = 0$. The turnover is the peak of the matter power spectrum.

Matter dependence

- The detection of the turnover scale (k_0) is highly sensitive to matter density. This makes it a valuable tool to constrain $\omega_m = \Omega_m h^2$.
- Besides this, the turnover scale is a potential standard candle of the universe [1].

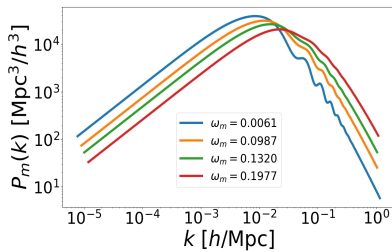


Figure 2: Shows the plot of the matter power spectrum plotted for different ω_m . Large values of ω_m , shift the turnover to small scales.

Checking the z -dependence

- An examination of the derivative of the matter power spectrum indicates that the turnover scale exhibits no redshift dependence.

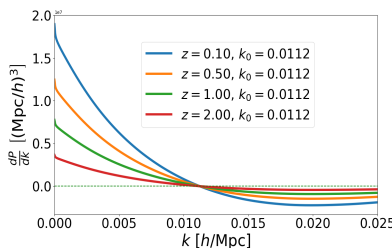


Figure 3: Shows the plot of the derivative of the matter power spectrum for different redshift values. All plots cross at the same point.

Models

- We model the HI IM power spectrum as

$$P_{\text{HI}}(k, \mu, z) = \bar{T}_{\text{HI}}^2(z) [b_{\text{HI}}(z) + f(z)\mu^2] P_m(k, z)$$
- Also, we model the effect of the foreground with

$$B_{\text{fg}}(k) = 1 - \exp\left[-\left(k_{\parallel}/k_{\parallel}^0\right)\right]$$
 and the effect of the telescope beam with

$$B_{\text{beam}}(k) = \exp\left[-\frac{1}{2}k_{\perp}^2 P_{\text{beam}}^2\right]$$
- For the turnover detection we make use of the model-independent parabolic fit for scales close to the turnover

$$\log_{10} P_{\text{HI}}(k) = \begin{cases} \log_{10}(P_0)(1 - \alpha x^2), & k < k_0 \\ \log_{10}(P_0)(1 - \beta x^2), & k \geq k_0 \end{cases}$$

where

$$x = \frac{\log_{10}(k[h/\text{Mpc}]) - \log_{10}(k_0[h/\text{Mpc}])}{\log_{10}(k_0[h/\text{Mpc}])}$$

Effects of foregrounds & beam

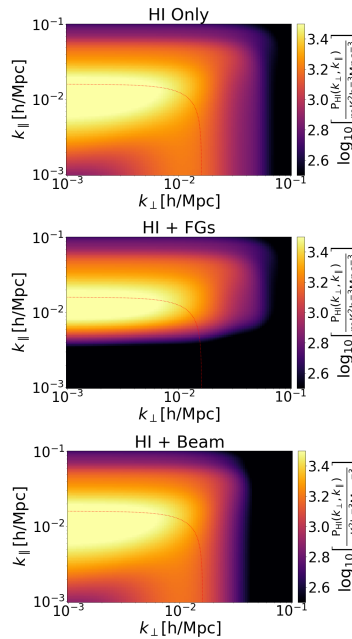


Figure 4: Shows the 2D HI IM power spectrum. The first plot shows the signal without any observational effects and the next plot displays the effects of foregrounds and that of the telescope beam. The brightest region is the location of the turnover, and thus, it is observed that the turnover scale is robust to IM observational effects.

Survey parameters

- We consider the following parameters for our IM surveys

Survey Parameters	MeerKCLASS		SKA-MID
	L-band	UHF-band	Band 1
Bandwidth [MHz]	ν_{min} 900 ν_{max} 1185*	580 1000	350 1050
Redshift range	z_{min} 0.2 z_{max} 0.58	0.4 1.45	0.35 3
Effective redshift	z_{eff} 0.39	0.925	1.675
Sky area [deg ²]	A_{sky} 4,000	4,000	20,000
Sky fraction	f_{sky} 0.10	0.10	0.48
Channel width [MHz]	$\delta\nu$ 0.2	0.2	0.2
Observation time [hrs]	t_{obs} 4,000	4,000	10,000
Number of dishes	N_{dish} 64	64	197
Dish diameter [m]	D_{dish} 13.5	13.5	15
Beam size (at z_{eff}) [deg]	θ_{FWHM} 1.5	1.7	2.6
Max scale [h/Mpc] $\times 10^3$	k_{min} 3.3	1.6	0.53

Expected performance

- The plots below unveil the anticipated error bars for our IM surveys.

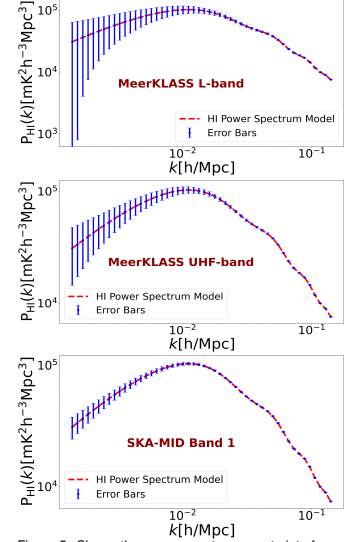


Figure 5: Shows the power spectrum constraints for our intensity mapping surveys. It can be observed that the MeerKCLASS L-band is going to struggle with detecting the turnover, but this is going to improve for the UHF-band. On the other hand, SKAO promises a high chance of turnover detection.

Results

- After fitting a parabolic curve to synthetic data, both MeerKCLASS bands were found to be consistent with the fiducial value of k_0 , and SKAO promises even tighter constraints [1].

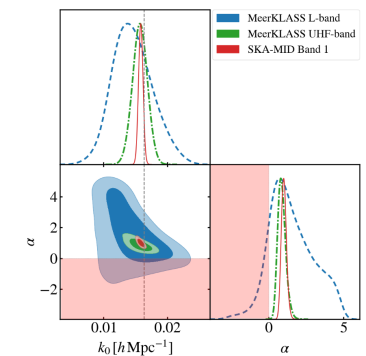


Figure 6: Shows the posterior values of the turnover scale and α .

Conclusions

- Recent findings by [1] reveal a 0.94σ detection significance with the MeerKAT L-band, which improves to 3.1σ for the MeerKAT UHF-band with a larger volume compared to the L-band. SKAO on the other hand achieves a 13.1σ detection.
- One goal of this project will be to verify these detection significances.

References

- [1] S. Cunnington. Detecting the power spectrum turnover with H I intensity mapping. *Mon. Not. Roy. Astron. Soc.*, 2022. <https://arxiv.org/abs/2202.13828>.
 [2] Berti et al. 21cm Intensity Mapping cross-correlation with galaxy surveys: current and forecasted cosmological parameters estimation for the SKAO. 2023. <https://arxiv.org/abs/2309.00710>.



Numerical construction of non linear initial data sets for cosmological models

A. Estrada Llesta¹, L. Dario Escobar²

¹ *Departament of Mathematics, University of Vienna*

² *Departament of Mathematics, Univeridad del Valle*

In this work, we explored the Algebraic-Hyperbolic Formulation (AHF) of the $2 + 1$ decomposition [1] of the constraint equations [2] in cosmological scenarios with a spatial topology of \mathbb{T}^3 . To do so, we proposed a pseudo-spectral method, based on the Fourier transform [3], to solve the system of PDEs in which the AHF rewrites the constraint equations. We successfully reproduced the analytical solutions for Gowdy [4] and Perturbed-FRW [5] spacetimes and found that the system exhibit a bad error behavior that is not aliasing-driven if the Y_i variables are not constant. To obtain new initial data sets, we proposed some modifications of the original AHF system that keep $Y_i = 0$ consistently. In particular, we explore two different ways in which is possible to reduce the $2 + 1$ system that allows us to obtain numerical solutions of the constraint equations with constraint violations under 10^{-10} .

- [1] István Rácz, *Class. and Quantum Grav.* **33** 015014 (2015).
- [2] Thomas W. Baumgarte, Stuart L. Shapiro, *Numerical Relativity. Solving Einstein's Equations on the Computer*, CAMBRIDGE UNIVERSITY PRESS (2010).
- [3] David A. Kopriva, *Implementing Spectral Methods for Partial Differential Equations*, Springer, Dordrecht (2009).
- [4] M. Alcubierre et. al., *Class. and Quantum Grav.* **21** 589 (2003).
- [5] CP. Ma and E. Bertschinger, *Astrophysical Journal*, **455** 7 (1995).

Abstract

TITLE: BINARY NEUTRON STAR SYSTEMS AS SUPER-EMITTERS OF GRAVITATIONAL WAVES.

AUTHOR: FIGUEROA HERNÁNDEZ, Juan Diego¹.

KEYWORDS: Gravitational waves, compact binary systems, neutron stars.

DESCRIPTION: In this work, we quantify the efficiency of gravitational wave emission during the merger process of compact objects, with a specific emphasis on binary neutron stars. Additionally, we determine the frequency range of the gravitational waves during the final stages of the merger. This enables us to infer the detectability of these systems by current terrestrial interferometers, such as LIGO-Virgo, as well as by future projects like the Einstein Telescope. To achieve this objective, we examine and extend approximate models already proposed in the literature. These models divide the merger into four main phases: i) adiabatic spiral regime, ii) plunge and merger, iii) damping or “ringdown” iv) final object: Kerr black hole or rapidly rotating neutron star. For the analysis and correspondence between the different phases, we use, in addition to the Newtonian formula for quadrupolar radiation, general laws of physics such as conservation of energy, conservation of angular momentum, conservation of baryonic matter, and quasi-universal relations describing the final neutron star that does not emit gravitational radiation. With this approach, we can discern which systems emit more energy per unit mass in the form of gravitational waves, i.e., which systems are super-emitters. Finally, we study the impact of the presence or absence of a disk around the final object and the effect of the rotation of the neutron stars forming the initial binary system. Approximate models following general laws of physics, such as the models in question, serve as guides for more detailed numerical investigations.

¹Universidad Industrial de Santander, Facultad de Ciencias, Escuela de Física, José Fernando Rodríguez Ruiz (Director), Laura Marcela Becerra Bayona (Co-directress), Luis Alberto Nuñez de Villavicencio (Co-director).

Abstract template for Summer School on Cosmology Poster Session

Gambardella Giosuè^{1,2}, Matteo Biagetti^{3,1,4}, Chiara Moretti^{4,7,1,5} and Emiliano Sefusatti^{5,1,6}

¹*Institute for Fundamental Physics of the Universe, Via Beirut 2, 34151 Trieste, Italy*

²*Institute of Space Sciences (ICE, CSIC), Campus UAB, Carrer de Can Magrans, s/n, 08193 Barcelona, Spain*

³*Area Science Park, Località Padriciano 99, 34149 Trieste, Italy*

⁴*Scuola Internazionale di Studi Superiori Avanzati, via Bonomea 265, 34136 Trieste, Italy*

⁵*Istituto Nazionale di Astrofisica, Osservatorio Astronomico di Trieste, via Tiepolo 11, 34143 Trieste, Italy*

⁶*Istituto Nazionale di Fisica Nucleare, Sezione di Trieste, via Valerio 2, 34127 Trieste, Italy*

⁷*Centro Nazionale “High Performance Computer, Big Data and Quantum Computing”*

We explore the reach of an analytical model at one-loop in Perturbation Theory (PT) to accurately describe measurements of the galaxy power spectrum from numerical simulations in redshift space. We consider the validity range in terms of three different diagnostics: 1) the goodness of fit; 2) a figure-of-bias quantifying the error in recovering the fiducial value of a cosmological parameter; 3) an internal consistency check of the theoretical model quantifying the running of the model parameters with the scale cut. We consider different sets of measurements corresponding to an increasing cumulative simulation volume in redshift space. For each volume we define a median value and the associated scatter for the largest wavenumber where the model is valid (the k -reach of the model). We find, as a rather general result, that the median value of the reach decreases with the simulation volume, as expected since the smaller statistical errors provide a more stringent test for the model. This is true for all the three definitions considered, with the one given in terms of the figure-of-bias providing the most stringent scale cut. More interestingly, we also find that the error associated with the k -reach value is quite large, with a significant probability of being as low as $0.1 h \text{Mpc}^{-1}$ (or, more generally, up to 40% smaller than the median) for all the simulation volumes considered. We explore as well the additional information on the growth rate parameter encoded in the power spectrum hexadecapole, compared to the analysis of monopole and quadrupole, as a function of simulation volume. While our analysis is, in many ways, rather simplified, we find that the gain in the determination of the growth rate is quite small in absolute value and well within the statistical error on the corresponding figure of merit.

Correlation between the X-ray morphology and the presence of diffuse radio emission sources in galaxy clusters.

Rupal Giri¹, Thomas Reiprich¹, and Florian Pacaud²

¹*Argelander Institute for Astronomy*


Galaxy cluster mergers are some of the most energetic phenomena in the universe. The dynamical state of clusters can hence be described as ‘relaxed/regular’ and ‘disturbed/merging’. These mergers tend to leave an imprint on the different components of the Intra-Cluster Medium (ICM). The spatial distribution of the X-ray flux of the cluster-wide, hot, optically thin thermal plasma is disrupted due to these mergers and can be characterized by an ‘irregular/disturbed’ morphology of the X-ray image. The small population of relativistic particles in the ICM, is also speculated to be energized due to shocks and turbulence generated during these mergers. These relativistic particles then emit synchrotron emission in the radio regime. This project aims to conduct a statistical study of the correlation between the X-ray morphology and the presence of the diffuse radio emission sources (radio halos and radio relics) in galaxy clusters using the X-ray-selected galaxy cluster sample eeHIFLUGCS. The study unveils that radio halo and radio relic sources have a statistically significant preference to be present in clusters that exhibit a ‘disturbed’ X-ray morphology. The morphological parameters concentration, X-ray centroid shift, and M_{20} (moment of the 20% brightest pixels in the X-ray image) are the most sensitive parameters to detect this preference. A disturbance measure ‘ D ’ is computed, as a combination of the three parameters to rank the galaxy clusters in the sample by their ‘disturbance level’. Additionally, the X-ray luminosity (L_X) of the host cluster and the radio luminosity of the radio halos (power at 1.4 GHz, $P_{1.4\text{GHz}}$) are observed to be correlated. Finally, it is discovered that the level of morphological disturbance (D) is correlated with radio luminosity residuals in the X-ray and radio luminosity correlation ($L_X - P_{1.4\text{GHz}}$), indicating the existence of more powerful radio halos in clusters that exhibit high levels of X-ray morphological disturbance.

Constraints on primordial black holes for nonstandard cosmologies

Tadeo D. Gomez-Aguilar¹, Luis E. Padilla¹, Encieh Erfani² and Juan Carlos Hidalgo¹

¹*Instituto de Ciencias Físicas, Universidad Nacional Autónoma de México, 62210, Cuernavaca, Morelos, México.*

²*PRISMA+ Cluster of Excellence & Mainz Institute for Theoretical Physics, Johannes Gutenberg-Universität Mainz, 55099 Mainz, Germany.*

We study how the bounds on the abundance of Primordial Black Holes (PBHs) and the constraints on power spectrum are modified if a non-standard evolution phase takes place between the end of inflation and the Standard radiation-dominated (RD) universe after inflation [1, 2]. The constraints on PBH abundance and power spectrum are computed using the new, freely available,  PBHBeta library, which accounts for the effects of non-standard expansion and specific criteria for PBH formation in such non-standard scenarios. As working examples, we consider three different cases: a pure matter-dominated (MD) phase, a scalar field-dominated (φ D) universe, and a stiff fluid-dominated (SD) scenario. While the background expansion is the same for the MD and φ D scenarios, the PBH formation criteria lead to different constraints to power spectrum. On the other hand, the duration of the non-standard expansion phase alters the bounds, with longer MD periods resulting in weaker constraints on power spectrum, and longer SD scenarios leading to an enhanced abundance due to the dust-like redshifting of PBHs. The modifications to the constraints are reported in all cases and we highlight those where the power spectrum may be significantly constrained.

An interesting extension for this work will be to explore the implications of time-dependent equations of state for the background, which may represent more realistic scenarios. For example, realistic models of the QCD transition, suggest a time-dependent equation of state, which is well-motivated by models of string cosmology [3]. It is important to assess whether PBHs could impose constraints on these models. Additionally, one could explore the production of gravitational waves and their evolution within nonstandard cosmologies (see for example [4]) or gravitational waves produced by the collision of PBHs, which persist after black hole evaporation. Such observables can be integrated into our set of constraints on ultra-light mass PBHs [5]. These and other extensions will be addressed in future work.

- [1] R. Allahverdi, M. A. Amin, A. Berlin, N. Bernal, C. T. Byrnes, M. S. Delos, A. L. Erickcek, M. Escudero, D. G. Figueroa, K. Freese, T. Harada, D. Hooper, D. I. Kaiser, T. Karwal, K. Kohri, G. Krnjaci, M. Lewicki, K. D. Lozanov, V. Poulin, K. Sinha, T. L. Smith, T. Takahashi, T. Tenkanen, J. Unwin, and S. Watson, “The First Three Seconds: a Review of Possible Expansion Histories of the Early Universe,” *The Open Journal of Astrophysics*, vol. 4, p. 1, Jan. 2021.
- [2] B. Carr, K. Kohri, Y. Sendouda, and J. Yokoyama, “Constraints on primordial black holes,” *Rept. Prog. Phys.*, vol. 84, no. 11, p. 116902, 2021.
- [3] C. P. Burgess, M. Cicoli, M. Gomez-Reino, F. Quevedo, G. Tasinato, and I. Zavala, “Non-standard primordial fluctuations and nongaussianity in string inflation,” *JHEP*, vol. 08, p. 045, 2010.
- [4] G. Domènech, “Induced gravitational waves in a general cosmological background,” *Int. J. Mod. Phys. D*, vol. 29, no. 03, p. 2050028, 2020.
- [5] T. Papanikolaou, V. Vennin, and D. Langlois, “Gravitational waves from a universe filled with primordial black holes,” *JCAP*, vol. 03, p. 053, 2021.

Abstract for Summer School on Cosmology Smr (3945)**Hugo Holland¹, Julien Grain¹***¹Institut d'Astrophysique Spatiale*

Primordial black holes could constitute part or all of dark matter but they require large inhomogeneities to form in the early universe. These inhomogeneities can strongly backreact on the large-scale dynamics of the universe. Stochastic inflation provides a way of studying this backreaction and getting an estimation of the abundance of primordial black holes. Because stochastic inflation focuses on large scale dynamics, it rests on the separate universe approach. However, the validity of this approach has only been checked in single field models [1], but not in multifield models in which we expect strong boosts in the power spectrum, leading to the formation of primordial black holes. We will check the validity of a separate universe approach in multifield models by matching it with a complete cosmological perturbation theory approach at large scales. In particular, we wish to compare these two paradigms and their differences in the adiabatic and entropic directions of the phase space. This will give us a range of validity and conditions one needs to verify in order to apply the separate universe approach and stochastic inflation in multifield models.

[1] D. Artigas, J. Grain, V. Vennin, JCAP 02 (2022), [2110.11720](#).

Abstract for ICTP Cosmology School Talk: Projection Bias in Optically Selected Galaxy Clusters for Euclid Survey

Roberto Ingrao^{1,2}, **Matteo Costanzi**^{1,2,3}, **Stefano Borgani**^{1,2,3,4,5}, **Tiago Castro**^{2,3,4,5} and **Alexandro Saro**^{1,2,3,4,5}

¹ *Astronomy Unit, Department of Physics, University of Trieste, via Tiepolo 11, I-34131 Trieste, Italy*

² *INAF-Osservatorio Astronomico di Trieste, via G. B. Tiepolo 11, I-34143 Trieste, Italy*

³ *Institute for Fundamental Physics of the Universe, Via Beirut 2, 34014 Trieste, Italy*

⁴ *INFN, Sezione di Trieste, Via Valerio 2, 34127 Trieste TS, Italy*

⁵ *ICSC - Italian Research Center on High-Performance Computing, Big Data and Quantum Computing*

Galaxy clusters are the most massive gravitationally bound objects in the Universe. Their number density offers a sensitive probe for growth rate of large scale structure and the underlying cosmology. A way to produce this type of analysis is relying on wide-field optical imaging and photometric surveys, since they are capable of providing both large cluster samples and weak gravitational lensing mass calibration. The combination of information from three cosmological observables such as cluster counts, clustering (i.e. 2-point correlation function) of clusters and weak lensing mass makes it possible to break some degeneracies between cosmological parameters and parameters defining scaling relations between lensing masses and richness, allowing for much more refined constraints on them via Bayesian inference techniques. In this scenario the photometric survey of galaxy clusters that is being carried out by the Euclid space telescope [1], will reach unprecedented sensitivity and, in turn, unprecedented precision on the expected constraints on cosmological parameters. In order to harvest the full potential of the Euclid's data a good understanding of the systematics is mandatory.

The work I will present, focus on the content of my Phd project, concentrating on the characterisation of the systematics related to projection effects and their impact on the scaling relation between weak lensing masses and observed richness of galaxy clusters to be identified in the Euclid wide survey. As already discussed in the literature [2], projection effects occur when multiple foreground and background objects along the same line of sight are mistakenly associated to a galaxy cluster, increasing the apparent richness of the cluster. While this effect is arguably of relative importance in the SDSS cluster survey, it has been shown to produce a significant effect on the cosmological posteriors derived from the Dark Energy Survey [3, 4]. We then expect that, if not accurately characterised, projection effects should have an even stronger impact in severely limiting the cosmological constraining power of the Euclid photometric cluster survey. In this optics, we propose to tackle this issue through a simulation based approach (similar to [5, 6]), generating mock catalogues capable of realistically capture the features of the upcoming Euclid Survey

[1] R. Laureijs et al., Euclid Definition Study Report, arXiv:1110.3193 (2011).

[2] A. Fumagalli et al., *Astronomy & Astrophysics*, Volume 682, id.A148, 16 pp., 7531 (2024).

[3] M. Costanzi et al., *Physical Review D*, Volume 103, Issue 4, article id.043522 (2021).

[4] Andrés N. Salcedo et al., *Dark Energy Survey Year 1 Clusters are Consistent with Planck*, arXiv:2310.03944, 7531 (2013).

[5] T. Sunayama, *Monthly Notices of the Royal Astronomical Society*, Volume 521, Issue 4, pp.5064-5076 (2023).

[6] H.-Y. Wu et al., *Monthly Notices of the Royal Astronomical Society*, Volume 515, Issue 3, pp.4471-4486 (2022).

Mixing bispectrum multipoles under geometric distortions

Giorgi Khomeriki^{1,4★} and Lado Samushia^{1,2,3}

¹1228 N. Martin Luther King Jr Drive, Department of Physics, Kansas State University, Manhattan, KS 66506-2601, USA

²45/57 Merab Kostava St, E. Kharadze Georgian National Astrophysical Observatory, 0179 Tbilisi, Georgia

³3/5 Cholokashvili Ave, School of Natural Sciences and Medicine, Ilia State University, Tbilisi 0162, Georgia

⁴9 Petre Chaikavskii St, I.Vekua School of Physics and Mathematics, 0108 Tbilisi, Georgia

Accepted 2023 October 27. Received 2023 October 19; in original form 2023 July 31

ABSTRACT

We derive general expressions for how the Alcock–Paczynski distortions affect the power spectrum and the bispectrum of cosmological fields. We compute explicit formulas for the mixing coefficients of bispectrum multipoles in the linear approximation. The leading-order effect for the bispectrum is the uniform dilation of all three wavevectors. The mixing coefficients depend on the shape of the bispectrum triplet. Our results for the bispectrum multipoles are framed in terms of the ‘natural’ basis of the lengths of three wavevectors but can be easily generalized for other bases and reduction schemes. Our validation tests confirm that the linear approximation is extremely accurate for all power spectrum multipoles. The linear approximation is accurate for the bispectrum monopole but results in sub-per cent level inaccuracies for the bispectrum quadrupole and fails for the bispectrum hexadecapole. Our results can be used to simplify the analysis of the bispectrum from galaxy surveys, especially the measurement of the baryon acoustic oscillation peak position. They can be used to replace numeric schemes with exact analytical formulae.

Key words: methods: analytical – cosmological parameters – distance scale – large-scale structure of the Universe.

1 INTRODUCTION

Galaxy surveys naturally record the positions of galaxies in spherical coordinates by measuring their angular positions and redshifts. We need to know the curvature of the Universe and its expansion history to convert these to Cartesian coordinates in physical units. If the fiducial model used for this conversion is offset from the real physics of the Universe, the distances between the galaxies will be distorted. These distortions can be used to derive the real cosmology from the fiducial model (Alcock & Paczynski 1979). This affects all statistical measures of the distribution of galaxies. For example, the measured power spectrum of galaxies will be a distorted version of the true power spectrum

$$P^m(k_{\parallel}k_{\perp}) = P^l(\alpha_{\parallel}[\mathbf{p}]k_{\parallel}^m, \alpha_{\perp}[\mathbf{p}]k_{\perp}^m), \quad (1)$$

where α_{\parallel} and α_{\perp} are the geometric distortion parameters along and across the line of sight that depend on cosmological parameters \mathbf{p} . If there is a feature in the power spectrum at a specific known wave number, these distortions can be used to constrain \mathbf{p} , by finding the values of α parameter that align the wavenumber of that feature to its known value in the measured power spectrum.

The geometric distortions are usually parametrized by α_V and α_{ϵ} , where the α_V parameter describes the average distortion of all the distances and the α_{ϵ} parameter describes the differential distortion of the line-of-sight distance with respect to the across-the-line-of-sight distances. Any measurement that has a feature at a known

scale will be sensitive to α_V and any measurement that is known to be isotropic (or if its angular anisotropy before the distortions is known accurately) will be sensitive to α_{ϵ} (Blake & Glazebrook 2003; Gaztañaga, Cabré & Hui 2009; Samushia et al. 2011; Kazin, Sánchez & Blanton 2012; Blazek et al. 2014; Song, Okumura & Taruya 2014; Ross, Percival & Manera 2015b; Sabiu & Song 2016; Melia & López-Corredoira 2017).

The baryon acoustic oscillation (BAO) feature is the most important distance scale that has been used in this fashion. The BAO is a pattern of overdensities in the initial distribution of matter (Cole et al. 2005; Eisenstein et al. 2005; Alam et al. 2017). The feature has been measured in the two-point clustering of many galaxy samples and these measurements provide the best current constrain on the distance redshift relationship (Ross et al. 2015a, 2017; du Mas des Bourboux et al. 2020; Bautista et al. 2021; Hou et al. 2021; Raichoor et al. 2021).

Other measurements that have been used for the same purpose include wavelet transformed galaxy fields (Valogiannis & Dvorkin 2022), cosmic void properties (Mao et al. 2017; Endo, Tashiro & Nishizawa 2020; Hamaus et al. 2022; Paz et al. 2023; Variu et al. 2023), void–galaxy clustering (Correa et al. 2019, 2022; Nadathur et al. 2019, 2020; Zhao et al. 2020; Woodfinden et al. 2022, 2023, 2023; Mauland et al. 2023; Paz et al. 2023; Radinović et al. 2023; Variu et al. 2023), Lyman α forest (Addison, Hinshaw & Halpern 2013; Cuceu et al. 2021, 2023), and HI intensity mapping (Naoz & Barkana 2008; Wyithe & Loeb 2009; Bernal et al. 2019; Wolz et al. 2019; Endo, Tashiro & Nishizawa 2020; Cunnington, Watkinson & Pourtsidou 2021; Soares et al. 2021; Rubiola, Cunnington & Camera 2022; Mauland et al.

* E-mail: giorgi.khomeriki@phys.ksu.edu

2023). Recent works suggested that the entire galaxy distribution can be used as a probe to measure the distortion parameters (Ramanah et al. 2019; Moriwaki, Nishimichi & Yoshida 2023).

The main objective of our work is to investigate the details of using galaxy bispectrum (three-point correlation function) multipoles for the same purpose. The bispectrum of galaxy density distribution, $B(k_1, k_2, k_3, \mu_1, \phi)$ is a function of five parameters (Scoccimarro 2000; Sefusatti et al. 2006). It is often expanded in the spherical harmonics, $B_{\ell m}(k_1, k_2, k_3)$, in its last two arguments for convenience (Gagrani & Samushia 2017; Sugiyama et al. 2019; Byun et al. 2021; Wang, Beutler & Sugiyama 2023; Sugiyama 2023a). Forecasts suggest that the bispectrum measurements can significantly enhance the cosmological constraints from the galaxy power spectrum (Gagrani & Samushia 2017; Yankelevich & Porciani 2019; Sugiyama et al. 2020; Mazumdar, Sarkar & Bharadwaj 2023; Tsedrik et al. 2023; Byun & Krause 2022). Recent works attempted to analyse galaxy bispectrum for measuring the BAO position (Slepian et al. 2017a, b; Pearson & Samushia 2018), and the full anisotropic shape (Scoccimarro 2004; Byun et al. 2017; Gil-Marín et al. 2017, 2018; Oddo et al. 2020, 2021; Moradinezhad Dizgah et al. 2021; Sugiyama et al. 2021, 2023a, b; Gualdi, Gil-Marín & Verde 2021b, b; Alkhanishvili et al. 2022; Philcox & Ivanov 2022; Mazumdar, Sarkar & Bharadwaj 2023; Rizzo et al. 2023), baryonic physics (Pollack, Smith & Porciani 2012; Slepian & Eisenstein 2015; Slepian et al. 2018; Yankelevich et al. 2023), and the primordial non-Gaussianity (Sefusatti & Komatsu 2007; Sefusatti, Crocce & Desjacques 2010; Figueroa et al. 2012; Byun et al. 2015; Maartens et al. 2021; Moradinezhad Dizgah et al. 2021; Clarke 2022; Goldstein et al. 2022; Giri, Münchmeyer & Smith 2023; Karagiannis et al. 2023; Coulton et al. 2023a, b). The clustering patterns of fourth and higher order have also been used in the analysis of galaxy samples (Fry & Peebles 1978; Verde & Heavens 2001; Philcox, Hou & Slepian 2021; Gualdi et al. 2021a; Gualdi, Gil-Marín & Verde 2021b; Gualdi & Verde 2022; Cahn & Slepian 2023; Hou, Slepian & Cahn 2023; Rizzo et al. 2023).

The geometric distortions mix the multipoles and this has to be accounted for in the analysis. The head-on solution is to model geometric distortions directly by rescaling the arguments of the measured bispectrum, but this is not computationally efficient. The power spectrum and the bispectrum are usually analysed by running Markov chain Monte Carlo (MCMC) over cosmological parameters (Handley, Hobson & Lasenby 2015; Zuntz et al. 2015; Brinckmann & Lesgourgues 2019; Torrado & Lewis 2021). Recomputing bispectrum models for each point in the MCMC chain is computationally expensive. A faster option is to estimate the distorted bispectrum from pre-computed moments and derivatives at a fiducial cosmology using a linear approximation. This is an established methodology for the power spectrum analysis (Padmanabhan & White 2008) and has also been used for the bispectrum analysis (Sugiyama et al. 2021).

After outlining basic formalism and establishing notation in Section 2, we provide a review of how the geometric distortions mix different power spectrum multipoles in Section 3. We then derive the mixing coefficients for the bispectrum multipoles in Section 4. The validity of linear expansion is tested in Section 5. We summarize our main findings in Section 6.

We assume the plain-parallel approximation throughout the paper (Matsubara 2000; Shiraiishi, Akitsu & Okumura 2021).

2 ALCOCK–PATCZYNSKI DISTORTIONS

We define the Alcock–Paczynski distortion parameters as

$$d_{\parallel} = \alpha_{\parallel} d_{\parallel}^t, \quad (2)$$

$$d_{\perp} = \alpha_{\perp} d_{\perp}^t. \quad (3)$$

They are related to the cosmological parameters through

$$\alpha_{\parallel} = \frac{H^t(z)}{H^{\text{fid}}(z)}, \quad (4)$$

$$\alpha_{\perp} = \frac{d_A^{\text{fid}}(z)}{d_A^t(z)}, \quad (5)$$

where $H(z)$ and $d_A(z)$ are the Hubble parameter and the angular diameter distance at redshift z . These distortions induce dual distortions in the Fourier space

$$k_{\parallel}^t = \alpha_{\parallel} k_{\parallel}, \quad (6)$$

$$k_{\perp}^t = \alpha_{\perp} k_{\perp}. \quad (7)$$

From now on, we will work with parameters

$$\alpha_V = \sqrt[3]{\alpha_{\perp}^2 \alpha_{\parallel}}, \quad (8)$$

$$\alpha_{\epsilon} = \sqrt[3]{\frac{\alpha_{\parallel}^2}{\alpha_{\perp}}}. \quad (9)$$

The definition of α_V is standard in the literature (Ballinger, Peacock & Heavens 1996). Our definition of α_{ϵ} differs from the established one ($\epsilon = \sqrt[3]{\alpha_{\parallel}/\alpha_{\perp}} - 1$). Either α_{ϵ} or ϵ can be used in analysis without a loss of information but we will later show that the definition of equation (9) has a clearer geometric meaning. To linear order, the two sets of distortion parameters are related as

$$\delta\alpha_V = \frac{1}{3} (\delta\alpha_{\parallel} + 2\delta\alpha_{\perp}), \quad (10)$$

$$\delta\alpha_{\epsilon} = \frac{2}{3} (\delta\alpha_{\parallel} - \delta\alpha_{\perp}). \quad (11)$$

Every wavevector's length and the angle with respect to the line-of-sight axis transform as

$$\begin{aligned} k^t &= k \sqrt{\mu^2(\alpha_{\parallel}^2 - \alpha_{\perp}^2) + \alpha_{\perp}^2} \\ &= k\alpha_V \sqrt{\mu^2(\alpha_{\epsilon}^2 - 1/\alpha_{\epsilon}) + 1/\alpha_{\epsilon}}, \end{aligned} \quad (12)$$

$$\begin{aligned} \mu^t &= \mu \frac{\alpha_{\parallel}}{\sqrt{\mu^2(\alpha_{\parallel}^2 - \alpha_{\perp}^2) + \alpha_{\perp}^2}} \\ &= \mu \frac{\alpha_{\epsilon}}{\sqrt{\mu^2(\alpha_{\epsilon}^2 - 1/\alpha_{\epsilon}) + 1/\alpha_{\epsilon}}}. \end{aligned} \quad (13)$$

To the linear order in AP parameters, this transformation is,

$$k^t = k [1 + \delta\alpha_V + L_2(\mu)\delta\alpha_{\epsilon}], \quad (14)$$

$$\mu^t = \mu \left[1 + \frac{3}{2} v^2 \delta\alpha_{\epsilon} \right]. \quad (15)$$

α_V is the average relative distortion of wavevector lengths over all possible directions and α_{ϵ} is the magnitude of the dipole distortion with respect to the line of sight. The angle of the wavevector is only affected by α_{ϵ} . This simple geometric meaning of the new distortion parameters is the motivation behind definitions of equations (8) and (9).

The bispectrum depends on three wavevectors that satisfy the condition $\mathbf{k}_1 + \mathbf{k}_2 + \mathbf{k}_3 = 0$. These three wavevectors are usually drawn to form a triangle to make this constraint more obvious.

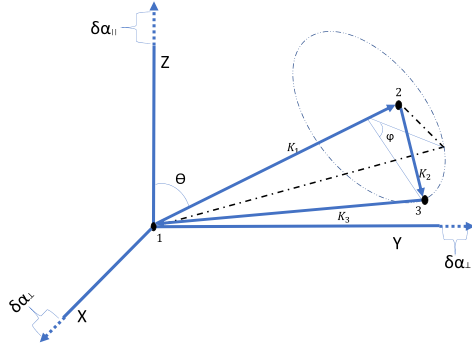


Figure 1. A depiction of three wavevectors defining a bispectrum and associated geometry. Points 1 and 2 are in the y - z plane.

The value of the bispectrum only depends on the lengths of the wavevectors k_1 , k_2 , k_3 , and their relative position with respect to the line-of-sight, which is usually parametrized by providing two numbers μ_1 and ϕ . μ_1 is the cosine of the k_1 with respect to the line of sight and ϕ is the angle of rotation of the triangle from the y - z plane.

Each of the three wavevectors scales by equations (14) and (15). We need to express the cosine and the sine of these wavevectors in terms of the five basic parameters k_1 , k_2 , k_3 , μ_1 , and ϕ to use these distortion formulae in our computations. These relationships turn out to be relatively simple.

$$\mu_1 = \mu_\theta, \quad (16)$$

$$\mu_2 = -\mu_{12}\mu_\theta + \mu_\phi v_{12}v_\theta, \quad (17)$$

$$\mu_3 = -\mu_{31}\mu_\theta - \mu_\phi v_{31}v_\theta, \quad (18)$$

where the subscripts 12 and 31 refer to the angles between wavevectors k_1 and k_2 , and k_3 and k_1 , respectively, and

$$\mu_{12} = \frac{\mathbf{k}_1 \cdot \mathbf{k}_2}{k_1 k_2}, \quad (19)$$

$$\mu_{31} = \frac{\mathbf{k}_3 \cdot \mathbf{k}_1}{k_3 k_1}. \quad (20)$$

The first relationship is obvious. The cosine of the angle of k_1 is one of the five basic parameters. The other two are derived in Appendix A. The true and the measured wavevector lengths are related by equations (12) and (13) for arbitrary distortions and by equations (14) and (15) for small distortions, with the angles from equations (16)–(18).

The angle ϕ also changes with distortions, but this has a subdominant effect on the multipoles and we ignore it in our computations.

Another effect of AP distortions is that all volumes are rescaled by a factor of $1/\alpha_v^3$. This results in a wavenumber-independent rescaling of the power spectrum by $1/\alpha_v^3$ and the bispectrum by a factor of $1/\alpha_v^6$. This is equivalent to the change of amplitude by $1-3\delta\alpha_v$ and $1-6\delta\alpha_v$ in the linear approximation. This rescaling of the amplitudes is simple enough that it should be modelled exactly even when the shape distortions are modelled in the linear approximation. We will not be including this overall rescaling factor in our formulae.

3 DISTORTIONS OF THE POWER SPECTRUM

The power spectrum is a function of a wavenumber length and its angle with respect to the line of sight and is usually expanded in

Table 1. All non-zero mixing coefficients for the power spectrum multipoles up to the fourth degree.

ℓ	ℓ'	$A_{\ell\ell'}$	$B_{\ell\ell'}$
0	2	$\frac{1}{5}$	$\frac{3}{5}$
2	0	1	0
2	2	$\frac{2}{7}$	$\frac{3}{7}$
2	4	$\frac{2}{7}$	$\frac{10}{7}$
4	2	$\frac{18}{35}$	$-\frac{36}{35}$
4	4	$\frac{20}{77}$	$\frac{30}{77}$

Legendre moments,

$$P(k, \mu) = \sum_l P_l(k) L_l(\mu). \quad (21)$$

The moments can be computed as

$$P_l(k) = \frac{2l+1}{2} \int d\mu P(k, \mu) L_l(\mu). \quad (22)$$

The AP distortions will distort the power spectrum,

$$P(k, \mu) = P^t(k^t[k, \mu], \mu^t[k, \mu]), \quad (23)$$

and its multipoles.

To linear order, the measured multipoles can be related to true multipoles as

$$P = P^t + \frac{\partial P^t}{\partial k} \left(\frac{\partial k}{\partial \alpha_v} \delta\alpha_v + \frac{\partial k}{\partial \alpha_\epsilon} \delta\alpha_\epsilon \right) + \frac{\partial P^t}{\partial \mu} \left(\frac{\partial \mu}{\partial \alpha_v} \delta\alpha_v + \frac{\partial \mu}{\partial \alpha_\epsilon} \delta\alpha_\epsilon \right). \quad (24)$$

Using equations (14) and (15), this becomes

$$P = P^t + \frac{\partial P^t}{\partial \ln k} \delta\alpha_v + \frac{\partial P^t}{\partial \ln k} L_2(\mu) \delta\alpha_\epsilon + \frac{\partial P^t}{\partial \ln \mu} \frac{3}{2} v^2 \delta\alpha_\epsilon. \quad (25)$$

For the multipoles we get,

$$P_\ell = \frac{2\ell+1}{2} \sum_{\ell'} \int d\mu \left[P_{\ell'}^t L_{\ell'}(\mu) + \frac{\partial P_{\ell'}^t}{\partial \ln k} L_{\ell'}(\mu) \delta\alpha_v + \frac{\partial P_{\ell'}^t}{\partial \ln k} L_{\ell'}(\mu) L_2(\mu) \delta\alpha_\epsilon + P_{\ell'}^t \frac{\partial L_{\ell'}(\mu)}{\partial \ln \mu} \frac{3}{2} v^2 \delta\alpha_\epsilon \right] L_\ell(\mu), \quad (26)$$

which results in

$$P_\ell = P_\ell^t + \frac{\partial P_\ell^t}{\partial \ln k} \delta\alpha_v + \sum_l \frac{\partial P_\ell^t}{\partial \ln k} A_{ll'} \delta\alpha_\epsilon + \sum_l P_l^t B_{ll'} \delta\alpha_\epsilon. \quad (27)$$

$$A_{ll'} = \frac{2\ell+1}{2} \int d\mu L_{\ell'}(\mu) L_\ell(\mu) L_2(\mu), \quad (28)$$

$$B_{ll'} = \frac{2\ell+1}{2} \int d\mu \frac{\partial L_{\ell'}(\mu)}{\partial \ln \mu} L_\ell(\mu) \frac{3}{2} v^2. \quad (29)$$

The leading order term stretches each multipole by a factor of $k\delta\alpha_v$, a constant fractional stretching by a factor of α_v for each wavenumber. The second and the third terms mix different multipoles and only depend on $\delta\alpha_\epsilon$. The mixing coefficients can be computed analytically and are given in Table 1 for the first four multipoles. Padmanabhan & White (2008) use the ϵ instead of α_ϵ so our coefficients need to be multiplied by two to match their formulas since to linear order $\delta\epsilon = 2\delta\alpha_\epsilon$.

4 DISTORTIONS OF THE BISPECTRUM

The bispectrum is a function of five parameters and is usually expanded in spherical multipoles,

$$B(k_1, k_2, k_3, \mu, \phi) = \sum_{\ell m} B_{\ell m}(k_1, k_2, k_3) Y_{\ell m}(\theta_1, \phi), \quad (30)$$

where $\theta_1 = \arccos(\mu_1)$. The multipoles can be computed via

$$B_{\ell m}(k_1, k_2, k_3) = \int d\mu_1 d\phi B(k_1, k_2, k_3, \mu_1, \phi) Y_{\ell m}(\theta_1, \phi). \quad (31)$$

The multipoles with non-zero m have negligible amplitudes and we will ignore the second index for the rest of the paper. The measured and the true bispectra are related by

$$B(k_1, k_2, k_3, \mu_1, \phi) = B^t(k_1^t, k_2^t, k_3^t, \mu_1^t, \phi^t), \quad (32)$$

where the right-hand side is implicitly a function of measured parameters through equations (12) and (13) with the angles given by equations (16)–(18). To linear order, the distortions are given by

$$\begin{aligned} B = B^t + \sum_{i=1,2,3} \frac{\partial B^t}{\partial k_i} \left(\frac{\partial k_i}{\partial \alpha_V} \delta \alpha_V + \frac{\partial k_i}{\partial \alpha_\epsilon} \delta \alpha_\epsilon \right) \\ + \frac{\partial B^t}{\partial \mu_1} \left(\frac{\partial \mu_1}{\partial \alpha_V} \delta \alpha_V + \frac{\partial \mu_1}{\partial \alpha_\epsilon} \delta \alpha_\epsilon \right) \\ + \frac{\partial B^t}{\partial \phi} \left(\frac{\partial \phi}{\partial \alpha_V} \delta \alpha_V + \frac{\partial \phi}{\partial \alpha_\epsilon} \delta \alpha_\epsilon \right). \end{aligned} \quad (33)$$

We checked that ϕ -derivatives have a subdominant effect and we will ignore them for the rest of the paper. Using equations (14) and (15), we get

$$\begin{aligned} B = B^t + \sum_{i=1,2,3} \frac{\partial B^t}{\partial \ln k_i} \delta \alpha_V + \sum_{i=1,2,3} \frac{\partial B^t}{\partial \ln k_i} L_2(\mu_i) \delta \alpha_\epsilon \\ + \frac{\partial B^t}{\partial \ln \mu_1} \frac{3}{2} v_1^2 \delta \alpha_\epsilon. \end{aligned} \quad (34)$$

Expanding both sides of the equation into multipoles results in

$$\begin{aligned} B_\ell = B_\ell^t + \sum_{i=1}^3 \frac{\partial B_\ell^t}{\partial \ln k_i} \delta \alpha_V + \sum_{\ell', m', i=1}^3 \frac{\partial B_{\ell' m'}^t}{\partial \ln k_i} C_{\ell \ell' m'}^{(i)} \delta \alpha_\epsilon \\ + \sum_{\ell'} \frac{\partial B_{\ell'}^t}{\partial \ln \mu_1} D_{\ell \ell'} \delta \alpha_\epsilon, \end{aligned} \quad (35)$$

where

$$C_{\ell \ell' m'}^{(i)} = \int d\mu_1 d\phi L_2(\mu_i) Y_{\ell 0}(\mu_1) Y_{\ell' m'}(\mu_1), \quad (36)$$

$$D_{\ell \ell'} = \frac{3}{2} \int d\mu_1 d\phi \frac{\partial Y_{\ell' m'}(\mu_1)}{\partial \ln \mu_1} v_1^2 Y_{\ell 0}(\mu_1). \quad (37)$$

The three leading terms tell us that, similarly to the power spectrum, all three wavevectors stretch with a relative scaling factor of $\delta \alpha_V$. The remaining terms mix the multipoles (including non-zero m multipoles). They can be computed analytically and their values are given in Tables 2 and 3. The C -coefficients are symmetric with respect to ℓ to ℓ' interchange, while the D -coefficients are not. These coefficients will have to be multiplied by a factor of 2 when using ϵ as the anisotropic warping parameter.

5 TESTING LINEAR APPROXIMATION

To test the validity of equations (27)–(29) and (35)–(37), we compute power spectrum and bispectrum in linear theory using Lambda cold

Table 2. All non-zero coefficients $C_{\ell \ell' m'}^{(i)}$ up to $\ell = 4$.

ℓ	ℓ'	m'	$C_{\ell \ell' m'}^{(1)}$	$C_{\ell \ell' m'}^{(2)}$	$C_{\ell \ell' m'}^{(3)}$
0	2	0	$\frac{1}{\sqrt{5}}$	$\frac{1}{\sqrt{5}} L_2(\mu_{12})$	$\frac{1}{\sqrt{5}} L(\mu_{31})$
0	2	2	0	$\frac{1}{2} \sqrt{\frac{3}{10}} v_{12}^2$	$\frac{1}{2} \sqrt{\frac{3}{10}} v_{31}^2$
2	0	0	$\frac{1}{\sqrt{5}}$	$\frac{1}{2\sqrt{5}} L_2(\mu_{12})$	$\frac{1}{2\sqrt{5}} L_2(\mu_{31})$
2	2	0	$\frac{2}{7}$	$\frac{2}{7} L_2(\mu_{12})$	$\frac{2}{7} L_2(\mu_{31})$
2	2	2	0	$-\frac{1}{7} \sqrt{\frac{3}{2}} v_{12}^2$	$-\frac{1}{7} \sqrt{\frac{3}{2}} v_{31}^2$
2	4	0	$\frac{6}{7\sqrt{5}}$	$\frac{6}{7\sqrt{5}} L_2(\mu_{12})$	$\frac{6}{7\sqrt{5}} L_2(\mu_{31})$
2	4	2	0	$\frac{3}{14\sqrt{2}} v_{12}^2$	$\frac{3}{14\sqrt{2}} v_{31}^2$
4	2	0	$\frac{6}{7\sqrt{5}}$	$\frac{6}{7\sqrt{5}} L_2(\mu_{12})$	$\frac{6}{7\sqrt{5}} L_2(\mu_{31})$
4	2	2	0	$\frac{1}{14} \sqrt{\frac{3}{10}} v_{12}^2$	$\frac{1}{14} \sqrt{\frac{3}{10}} v_{31}^2$
4	4	0	$\frac{20}{77}$	$\frac{20}{77} L_2(\mu_{12})$	$\frac{20}{77} L_2(\mu_{31})$
4	4	2	0	$-\frac{9}{77} \sqrt{\frac{5}{2}} v_{12}^2$	$-\frac{9}{77} \sqrt{\frac{5}{2}} v_{31}^2$
4	6	0	$\frac{15}{11\sqrt{13}}$	$\frac{15}{11\sqrt{13}} L_2(\mu_{12})$	$\frac{15}{11\sqrt{13}} L_2(\mu_{31})$
4	6	2	0	$\frac{1}{22} \sqrt{\frac{105}{13}} v_{12}^2$	$\frac{1}{22} \sqrt{\frac{105}{13}} v_{31}^2$

Table 3. All non-zero $D_{\ell \ell'}$ coefficients up to $\ell = 4$.

ℓ	ℓ'	$D_{\ell \ell'}$
0	2	$\frac{3}{\sqrt{5}}$
2	2	$\frac{3}{7}$
2	4	$\frac{6}{7\sqrt{5}}$
4	2	$-\frac{12}{7\sqrt{5}}$
4	4	$\frac{30}{77}$
4	6	$\frac{105}{11\sqrt{13}}$

dark matter model (see Appendix C) with best-fitting parameters as constrained by the *Planck* satellite mission (Planck Collaboration VI 2020). We first compute the power spectrum by distorting the wavenumbers following the exact formula in equation (23). We then compute the linear approximation of equation (27). The ratio of these two computations to the undistorted power spectrum is shown in Fig. 2. We make our computations for a 1 per cent offset in α_V and α_ϵ . If the templates are closer, the agreement between the linear approximation and the full computations is obviously better.

The figure shows the ratios for the first three even multipoles of the power spectrum in the wavelength range $0 < k < 0.2 h^{-1} \text{Mpc}$. α_V has a significantly larger effect on the monopole than the α_ϵ for the same level of distortion. A one per cent deviation in α_V results in about a two per cent deviation in the monopole amplitude, with a clearly visible BAO signature. The linear approximation is in excellent agreement with the exact result. α_V -distortions are smaller than α_ϵ -distortions in the quadrupole, but they are not negligible. A one per cent distortion in α_ϵ results in a six per cent offset in the original amplitude of the quadrupole, while a similar distortion in the α_V results in a two per cent offset. Both distortions have clear BAO signals imprinted in them. α_ϵ -distortions dominate the quadrupole. A one per cent offset in α_ϵ results in up to 30 per cent offset in the quadrupole amplitude. The linear approximation works exceedingly well for all three multipoles.

Fig. 3 shows a similar ratio for the bispectrum. The bispectrum monopole is completely dominated by the α_V -distortions.

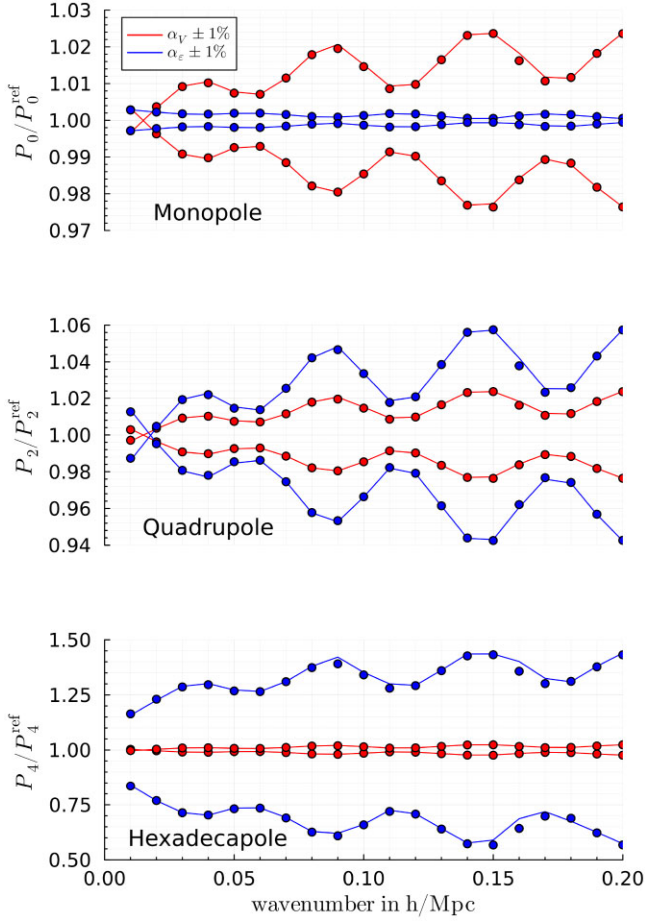


Figure 2. The ratio of distorted power spectrum multipoles to the fiducial (undistorted) ones. The points represent the results from the exact formula, while the lines represent the computations based on the linear approximation. The panels show the monopole, the quadrupole, and the hexadecapole of the power spectrum from top to bottom, respectively. Red data points and lines correspond to a one per cent offset in α_V , while the blue data points and lines correspond to a one per cent offset in α_ϵ .

One per cent offset in α_V results in a four per cent offset in the monopole amplitude, and the BAO feature is clearly pronounced. α_ϵ and α_V distortions have comparable effects on the bispectrum quadrupole, both resulting in a four per cent offset of the amplitude for one per cent distortion. The linear approximation works extremely well for the bispectrum monopole. We start seeing some deviation between the linear prediction and the exact result for the bispectrum quadrupole at low wavevectors. This deviation is mostly in amplitude and preserves the position of the BAO peaks. The deviation is larger at small wavenumbers where the relative distortions caused by α_ϵ are larger. The bispectrum hexadecapole is extremely strongly affected by the α_ϵ -distortions and the linear expansion fails even for small distortions. Fig. 4 shows the effect of a one per cent distortion in the bispectrum hexadecapole. The amplitude of hexadecapole changes by a factor of 2 even for such a small distortion.

6 CONCLUSIONS

We derived explicit analytical expressions for the mixing coefficients of the bispectrum multipoles to the linear order in Alcock–Paczynski distortions. They are presented in Tables 2 and 3 for the multipoles up to $\ell = 4$. The coefficients are derived for the natural definition

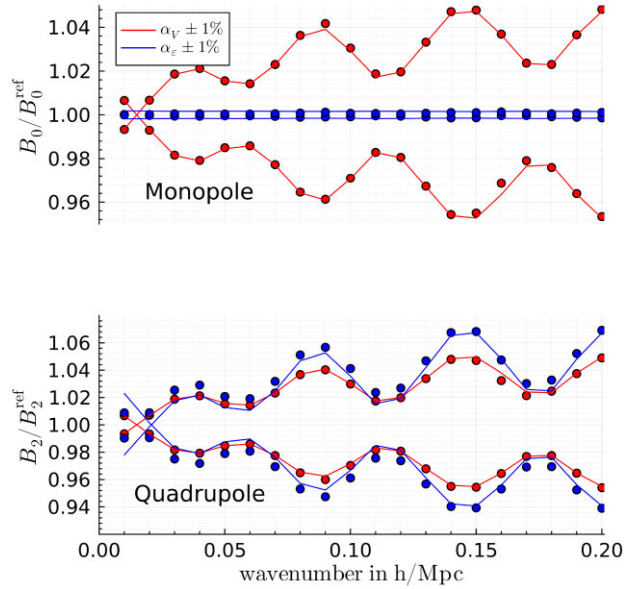


Figure 3. The ratio of distorted bispectrum multipoles to the fiducial (undistorted) ones. The points represent the results from the exact formula, while the lines represent the computations based on the linear approximation. The panels show the monopole and the quadrupole of the bispectrum from top to bottom respectively. Red data points and lines correspond to a one per cent offset in α_V , while the blue data points and lines correspond to a one per cent offset in α_ϵ .

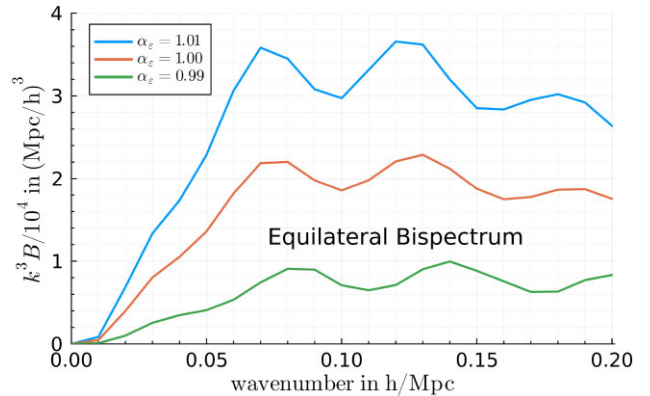


Figure 4. Response of the bispectrum hexadecapole (equilateral configuration) to a one per cent offset in α_ϵ .

of the bispectrum multipoles but can easily be extended to other parametrizations and definitions (e.g. the ones proposed in Gualdi et al. 2019; Sugiyama et al. 2019). We find that the linear order mixing coefficients work extremely well for all power spectrum multipoles (see Fig. 2). For the bispectrum monopole, the leading order mixing model works very well. The isotropic stretching (non-zero α_V) is modelled very accurately by the linear expression for all multipoles. The linear mixing model is not so accurate for the anisotropic stretching (non-zero α_ϵ ; see Fig. 3). Predictions for the bispectrum quadrupole deviate by a fraction of a per cent for $\alpha_\epsilon \sim 1$ per cent. Even small values of $\alpha_\epsilon \sim 1$ per cent induce large changes in the amplitude and shape of the bispectrum hexadecapole and the linear approximation obviously fails. So, generally speaking, the good agreement between the linear approximation and the exact full model is not guaranteed. Our work shows that using linear

approximation for bispectrum multipoles, while resulting in great improvement in computational speed, needs to be done carefully. Fiducial templates used in computation must not be very far (in terms of the α_ϵ values) from the measurements. Exactly how close they need to be depends on the strength of the bispectrum monopole signal and will vary from sample to sample. Our findings will be helpful for future analysis of galaxy bispectrum, especially for the works that aim to measure the BAO feature in the galaxy bispectrum. The computational cost of modelling AP distortions of the bispectrum monopole and quadrupole can be significantly reduced by using the linear mixing model around a fiducial value as opposed to directly computing the distorted monopoles. The linear mixture model does not seem to be sufficiently accurate for the bispectrum quadrupole and computationally more expensive, direct computation may be unavoidable.

ACKNOWLEDGEMENTS

The authors are grateful for the support from the U.S. Department of Energy via grants DE-SC0021165 and DE-SC0011840. LS is grateful for support from the NASA ROSES grant 12-EUCLID12-0004 and the Shota Rustaveli National Science Foundation of Georgia grants FR 19–498.

The authors thank the unanimous referee for very valuable comments.

DATA AVAILABILITY

The code used to make figures in this manuscript is available at <https://github.com/ladosamushia/BispectrumAP>.

REFERENCES

- Addison G. E., Hinshaw G., Halpern M., 2013, *MNRAS*, 436, 1674
- Alam S. et al., 2017, *MNRAS*, 470, 2617
- Alcock C., Paczynski B., 1979, *Nature*, 281, 358
- Alkhanishvili D., Porciani C., Sefusatti E., Biagetti M., Lazanu A., Oddo A., Yankelevich V., 2022, *MNRAS*, 512, 4961
- Ballinger W. E., Peacock J. A., Heavens A. F., 1996, *MNRAS*, 282, 877
- Bautista J. E. et al., 2021, *MNRAS*, 500, 736
- Bernal J. L., Breyse P. C., Gil-Marín H., Kovetz E. D., 2019, *Phys. Rev. D*, 100, 123522
- Blake C., Glazebrook K., 2003, *ApJ*, 594, 665
- Blazek J., Seljak U., Vlah Z., Okumura T., 2014, *J. Cosmol. Astropart. Phys.*, 2014, 001
- Brinckmann T., Lesgourgues J., 2019, *Phys. Dark Universe*, 24, 100260
- Byun J., Krause E., 2022, *MNRAS*, 525, 4854
- Byun J., Agarwal N., Bean R., Holman R., 2015, *Phys. Rev. D*, 91, 123518
- Byun J., Eggemeier A., Regan D., Seery D., Smith R. E., 2017, *MNRAS*, 471, 1581
- Byun J., Oddo A., Porciani C., Sefusatti E., 2021, *J. Cosmol. Astropart. Phys.*, 2021, 105
- Cahn R. N., Slepian Z., 2023, *J. Phys. A: Math. Theor.*, 56, 325204
- Clarke P., 2022, PhD thesis, Univ. Cambridge
- Cole S. et al., 2005, *MNRAS*, 362, 505
- Correa C. M., Paz D. J., Padilla N. D., Ruiz A. N., Angulo R. E., Sánchez A. G., 2019, *MNRAS*, 485, 5761
- Correa C. M., Paz D. J., Padilla N. D., Sánchez A. G., Ruiz A. N., Angulo R. E., 2022, *MNRAS*, 509, 1871
- Coulton W. R. et al., 2023a, *ApJ*, 943, 64
- Coulton W. R. et al., 2023b, *ApJ*, 943, 178
- Cuceu A., Font-Ribera A., Joachimi B., Nadathur S., 2021, *MNRAS*, 506, 5439
- Cuceu A. et al., 2023, *MNRAS*, 523, 3773
- Cunnington S., Watkinson C., Pourtsidou A., 2021, *MNRAS*, 507, 1623
- du Mas des Bourboux H. et al., 2020, *ApJ*, 901, 153
- Eisenstein D. J. et al., 2005, *ApJ*, 633, 560
- Endo T., Tashiro H., Nishizawa A. J., 2020, *MNRAS*, 499, 587
- Figueroa D. G., Sefusatti E., Riotto A., Vernizzi F., 2012, *J. Cosmol. Astropart. Phys.*, 2012, 036
- Fry J. N., Peebles P. J. E., 1978, *ApJ*, 221, 19
- Gagrani P., Samushia L., 2017, *MNRAS*, 467, 928
- Gaztañaga E., Cabré A., Hui L., 2009, *MNRAS*, 399, 1663
- Gil-Marín H., Percival W. J., Verde L., Brownstein J. R., Chuang C.-H., Kitaura F.-S., Rodríguez-Torres S. A., Olmstead M. D., 2017, *MNRAS*, 465, 1757
- Gil-Marín H. et al., 2018, *MNRAS*, 477, 1604
- Giri U., Münchmeyer M., Smith K. M., 2023, preprint (arXiv:2305.03070)
- Goldstein S., Esposito A., Philcox O. H. E., Hui L., Hill J. C., Scoccimarro R., Abitbol M. H., 2022, *Phys. Rev. D*, 106, 123525
- Gualdi D., Verde L., 2022, *J. Cosmol. Astropart. Phys.*, 2022, 050
- Gualdi D., Gil-Marín H., Manera M., Joachimi B., Lahav O., 2019, *MNRAS*, 484, L29
- Gualdi D., Novell S., Gil-Marín H., Verde L., 2021a, *J. Cosmol. Astropart. Phys.*, 2021, 015
- Gualdi D., Gil-Marín H., Verde L., 2021b, *J. Cosmol. Astropart. Phys.*, 2021, 008
- Hamaus N. et al., 2022, *A&A*, 658, A20
- Handley W. J., Hobson M. P., Lasenby A. N., 2015, *MNRAS*, 453, 4384
- Hou J. et al., 2021, *MNRAS*, 500, 1201
- Hou J., Slepian Z., Cahn R. N., 2023, *MNRAS*, 522, 5701
- Karagiannis D., Maartens R., Fonseca J., Camera S., Clarkson C., 2023, preprint (arXiv:2305.04028)
- Kazin E. A., Sánchez A. G., Blanton M. R., 2012, *MNRAS*, 419, 3223
- Lewis A., Bridle S., 2002, *Phys. Rev. D*, 66, 103511
- Maartens R., Jolicoeur S., Umeh O., De Weerd E. M., Clarkson C., 2021, *J. Cosmol. Astropart. Phys.*, 2021, 013
- Mao Q., Berlind A. A., Scherrer R. J., Neyrinck M. C., Scoccimarro R., Tinker J. L., McBride C. K., Schneider D. P., 2017, *ApJ*, 835, 160
- Matsubara T., 2000, *ApJ*, 535, 1
- Mauland R., Elgarøy Ø., Mota D. F., Winther H. A., 2023, *A&A*, 674, A185
- Mazumdar A., Sarkar D., Bharadwaj S., 2023, *MNRAS*, 520, 2534
- Melia F., López-Corredoira M., 2017, *Int. J. Mod. Phys. D*, 26, 1750055
- Moradinezhad Dizgah A., Biagetti M., Sefusatti E., Desjacques V., Noreña J., 2021, *J. Cosmol. Astropart. Phys.*, 2021, 015
- Moriwaki K., Nishimichi T., Yoshida N., 2023, *Rep. Prog. Phys.*, 86, 076901
- Nadathur S., Carter P. M., Percival W. J., Winther H. A., Bautista J. E., 2019, *Phys. Rev. D*, 100, 023504
- Nadathur S., Percival W. J., Beutler F., Winther H. A., 2020, *Phys. Rev. Lett.*, 124, 221301
- Naoz S., Barkana R., 2008, *MNRAS*, 385, L63
- Oddo A., Sefusatti E., Porciani C., Monaco P., Sánchez A. G., 2020, *J. Cosmol. Astropart. Phys.*, 2020, 056
- Oddo A., Rizzo F., Sefusatti E., Porciani C., Monaco P., 2021, *J. Cosmol. Astropart. Phys.*, 2021, 038
- Padmanabhan N., White M., 2008, *Phys. Rev. D*, 77, 123540
- Paz D. J., Correa C. M., Gualpa S. R., Ruiz A. N., Bederián C. S., Graña R. D., Padilla N. D., 2023, *MNRAS*, 522, 2553
- Pearson D. W., Samushia L., 2018, *MNRAS*, 478, 4500
- Philcox O. H. E., Ivanov M. M., 2022, *Phys. Rev. D*, 105, 043517
- Philcox O. H. E., Hou J., Slepian Z., 2021, preprint (arXiv:2108.01670)
- Planck Collaboration VI, 2020, *A&A*, 641, A6
- Pollack J. E., Smith R. E., Porciani C., 2012, *MNRAS*, 420, 3469
- Radinović S. et al., 2023, *A&A*, 677, A78
- Raichoor A. et al., 2021, *MNRAS*, 500, 3254
- Ramanah D. K., Lavaux G., Jasche J., Wandelt B. D., 2019, *A&A*, 621, A69
- Rizzo F., Moretti C., Pardede K., Eggemeier A., Oddo A., Sefusatti E., Porciani C., Monaco P., 2023, *J. Cosmol. Astropart. Phys.*, 2023, 031
- Ross A. J., Samushia L., Howlett C., Percival W. J., Burden A., Manera M., 2015a, *MNRAS*, 449, 835
- Ross A. J., Percival W. J., Manera M., 2015b, *MNRAS*, 451, 1331
- Ross A. J. et al., 2017, *MNRAS*, 464, 1168

- Rubiola A., Cunnington S., Camera S., 2022, *MNRAS*, 516, 5454
 Sabiu C. G., Song Y.-S., 2016, preprint (arXiv:1603.02389)
 Samushia L. et al., 2011, *MNRAS*, 410, 1993
 Scoccimarro R., 2000, *ApJ*, 544, 597
 Scoccimarro R., 2004, *Phys. Rev. D*, 70, 083007
 Sefusatti E., Komatsu E., 2007, *Phys. Rev. D*, 76, 083004
 Sefusatti E., Crocce M., Pueblas S., Scoccimarro R., 2006, *Phys. Rev. D*, 74, 023522
 Sefusatti E., Crocce M., Desjacques V., 2010, *MNRAS*, 406, 1014
 Shiraishi M., Akitsu K., Okumura T., 2021, *Phys. Rev. D*, 103, 123534
 Slepian Z., Eisenstein D. J., 2015, *MNRAS*, 448, 9
 Slepian Z. et al., 2017a, *MNRAS*, 468, 1070
 Slepian Z. et al., 2017b, *MNRAS*, 469, 1738
 Slepian Z. et al., 2018, *MNRAS*, 474, 2109
 Soares P. S., Cunnington S., Pourtsidou A., Blake C., 2021, *MNRAS*, 502, 2549
 Song Y.-S., Okumura T., Taruya A., 2014, *Phys. Rev. D*, 89, 103541
 Sugiyama N. S., Saito S., Beutler F., Seo H.-J., 2019, *MNRAS*, 484, 364
 Sugiyama N. S., Saito S., Beutler F., Seo H.-J., 2020, *MNRAS*, 497, 1684
 Sugiyama N. S., Saito S., Beutler F., Seo H.-J., 2021, *MNRAS*, 501, 2862
 Sugiyama N. S. et al., 2023a, *MNRAS*, 523, 3133
 Torrado J., Lewis A., 2021, *J. Cosmol. Astropart. Phys.*, 2021, 057
 Tsedrik M., Moretti C., Carrilho P., Rizzo F., Pourtsidou A., 2023, *MNRAS*, 520, 2611
 Valogiannis G., Dvorkin C., 2022, *Phys. Rev. D*, 106, 103509
 Variu A., Zhao C., Forero-Sánchez D., Chuang C.-H., Kitaura F.-S., Tao C., Tamone A., Kneib J.-P., 2023, *MNRAS*, 521, 4731
 Verde L., Heavens A. F., 2001, *ApJ*, 553, 14
 Wang M. S., Beutler F., Sugiyama N. S., 2023, preprint (arXiv:2304.03643)
 Wolz L., Murray S. G., Blake C., Wyithe J. S., 2019, *MNRAS*, 484, 1007
 Woodfinden A., Nadathur S., Percival W. J., Radinovic S., Massara E., Winther H. A., 2022, *MNRAS*, 516, 4307
 Woodfinden A., Percival W. J., Nadathur S., Winther H. A., Fraser T. S., Massara E., Paillas E., Radinovic S., 2023, *MNRAS*, 523, 6360
 Wyithe J. S. B., Loeb A., 2009, *MNRAS*, 397, 1926
 Yankelevich V., Porciani C., 2019, *MNRAS*, 483, 2078
 Yankelevich V., McCarthy I. G., Kwan J., Stafford S. G., Liu J., 2023, *MNRAS*, 521, 1448
 Zhao C. et al., 2020, *MNRAS*, 491, 4554
 Zuntz J. et al., 2015, *Astron. Comput.*, 12, 45

APPENDIX A: WAVEVECTOR PROJECTIONS

Our goal is to derive expressions for the cosine of the angle with respect to the z -axis for an arbitrary triangle shown in Fig. 1.

We will start with a triangle in the y - z plane with a \mathbf{k}_1 vector along the positive y -axis. To get the triangle in Fig. B1, we have to rotate the initial triangle by angle ϕ counterclockwise with respect to the y -axis and by the angle $\pi/2 - \theta_1$ counterclockwise with respect to the x -axis.

Matrices corresponding to these rotations are

$$\mathbf{R}_y = \begin{pmatrix} \cos(\phi) & 0 & \sin(\phi) \\ 0 & 1 & 0 \\ -\sin(\phi) & 0 & \cos(\phi) \end{pmatrix}, \quad (\text{A1})$$

and

$$\mathbf{R}_x = \begin{pmatrix} 1 & 0 & 0 \\ 0 & \sin(\theta) & -\cos(\theta) \\ 0 & \cos(\theta) & \sin(\theta) \end{pmatrix}. \quad (\text{A2})$$

The initial positions of wavevectors are

$$\mathbf{k}_{1,\text{ini}} = (0, k_1, 0)^T, \quad (\text{A3})$$

$$\mathbf{k}_{2,\text{ini}} = (0, -k_2\mu_{12}, k_2\nu_{12})^T, \quad (\text{A4})$$

$$\mathbf{k}_{3,\text{ini}} = (0, -k_3\mu_{31}, -k_3\nu_{31})^T, \quad (\text{A5})$$

where θ_{ij} is the angle between vectors \mathbf{k}_i and \mathbf{k}_j .

After the rotation, we get

$$\mathbf{k}_1 = R_x R_y \mathbf{k}_{1,\text{ini}} = (0, k_1\nu_\theta, k_1\mu_\theta)^T,$$

$$\mathbf{k}_2 = R_x R_y \mathbf{k}_{2,\text{ini}} = (k_2\nu_{12}\nu_\theta, -k_2\mu_\theta\mu_\phi\nu_{12} - k_2\mu_{12}\nu_\theta, -k_2\mu_{12}\mu_\theta + k_2\mu_\phi\nu_{12}\nu_\theta)^T,$$

$$\mathbf{k}_3 = R_x R_y \mathbf{k}_{3,\text{ini}} = (-k_3\nu_{31}\nu_\theta, k_3\mu_\theta\mu_\phi\nu_{31} - k_3\mu_{31}\nu_\theta, -k_3\mu_{31}\mu_\theta - k_3\mu_\phi\nu_{31}\nu_\theta)^T,$$

and the cosine of the angle with respect to the line of sight is

$$\mu_1 = \mu_\theta, \quad (\text{A7})$$

$$\mu_2 = -\mu_{12}\mu_\theta + \mu_\phi\nu_{12}\nu_\theta, \quad (\text{A8})$$

$$\mu_3 = -\mu_{31}\mu_\theta - \mu_\phi\nu_{31}\nu_\theta. \quad (\text{A9})$$

APPENDIX B: BISPECTRUM PROJECTIONS FROM GEOMETRY

The results in Appendix A can also be derived using simple Euclidean geometry. The angle and the magnitude of \mathbf{k}_1 are trivial. For the other two wavevectors, we get the following expressions.

$$k_2^1 = \sqrt{k_2^2 + (\alpha_{\parallel} - 1)^2 k_1 \mu} - k_3 \sqrt{1 - \frac{r^2 v_\phi^2}{k_3^2} \cos(\alpha_\epsilon^\phi + \theta)^2 + (\alpha_\perp - 1)^2 (k_1 v - k_3 \sqrt{1 - \frac{r^2 v_\phi^2}{k_3^2} \sin(\alpha_\epsilon^\phi + \theta)^2 + \frac{r^2 v_\phi^2}{k_3} (\alpha_\perp - 1)^2}} \quad (\text{B1})$$

$$k_3^1 = k_3 \sqrt{\left(1 - \frac{r^2 \sin^2 \phi}{k_3^2}\right) \left[\cos^2(\alpha_\epsilon^\phi + \theta) \alpha_{\parallel}^2 + \sin^2(\alpha_\epsilon^\phi + \theta) \alpha_{\perp}^2\right] + \frac{r^2 \sin^2 \phi}{k_3^2} \alpha_{\perp}^2}, \quad (\text{B2})$$

where

$$\alpha_\epsilon^\phi = \arctan\left(\frac{r \cos \phi}{d}\right) \quad (\text{B3})$$

and

$$\xi^\phi = \arctan\left(\frac{r \cos \phi}{k_1 - d}\right) \quad (\text{B4})$$

To linear order in small distortions, these become

$$k_2^1 = k_2 + \delta\alpha_{\parallel} \left[k_1 \mu - k_3 \sqrt{1 - \frac{r^2 \sin^2 \phi}{k_3^2} \cos(\alpha_\epsilon^\phi + \theta)} \right] + \delta\alpha_{\perp} \left[k_1 v - k_3 \sqrt{1 - \frac{r^2 \sin^2 \phi}{k_3^2} \sin(\alpha_\epsilon^\phi + \theta)} \right] + \delta\alpha_{\perp} \frac{r^2 \sin^2 \phi}{k_2} \quad (\text{B5})$$

$$k_3^1 = k_3 \left(1 - \frac{r^2 \sin^2 \phi}{k_3^2}\right) \left[\cos^2(\alpha_\epsilon^\phi + \theta) \delta\alpha_{\parallel} + \sin^2(\alpha_\epsilon^\phi + \theta) \delta\alpha_{\perp}\right] + k_3 \frac{r^2 \sin^2 \phi}{k_3^2} \delta\alpha_{\perp} + k_3 \quad (\text{B6})$$

Distortions in ϕ are given by

$$\phi^1 = \text{asin}\left(\frac{r}{r^1} \sin \phi (1 + \delta\alpha_{\perp})\right), \quad (\text{B7})$$

where

$$r = \sqrt{k_3^2 - d^2}, \quad (\text{B8})$$

and

$$d = \frac{k_1^2 + k_3^2 - k_2^2}{2k_1}. \quad (\text{B9})$$

The distortions in r to linear order are

$$\frac{r}{r^1} = 1 + \delta k_1 - \frac{1}{r^2 k_1^2} \left[\sum_{i,j}^{i \neq j} k_i^2 k_j^2 \delta k_j - \sum_{i=1}^3 k_i^4 \delta k_i \right], \quad (\text{B10})$$

which results in the following linearized expression for the ϕ :

$$\phi^1 = \phi + \tan \phi \left(\delta\alpha_{\perp} + \delta k_1 - \frac{1}{r^2 k_1^2} \left[\sum_{i,j}^{i \neq j} k_i^2 k_j^2 \delta k_j - \sum_{i=1}^3 k_i^4 \delta k_i \right] \right). \quad (\text{B11})$$

For equilateral configurations, with $k_1 = k_2 = k_3 = K$, the equations above simplify further to

$$k_1^1 = K(1 + \mu^2 \delta\alpha_{\parallel} + v^2 \delta\alpha_{\perp}), \quad (\text{B12})$$

$$k_2^1 = K + \delta\alpha_{\parallel} \left[K\mu - K \sqrt{1 - \frac{3 \sin^2 \phi}{4}} \left(\frac{\mu}{\sqrt{1 + 3 \cos^2 \phi}} - \frac{v\sqrt{3} \cos \phi}{\sqrt{1 + 3 \cos^2 \phi}} \right) \right] + \delta\alpha_{\perp} \left[K v - K \sqrt{1 - \frac{3 \sin^2 \phi}{4}} \left(\frac{\mu\sqrt{3} \cos \phi}{\sqrt{1 + 3 \cos^2 \phi}} + \frac{v}{\sqrt{1 + 3 \cos^2 \phi}} \right) \right] + \delta\alpha_{\perp} K \frac{\sin^2 \phi}{4}, \quad (\text{B13})$$

$$k_3^1 = K + K \left(1 - \frac{3 \sin^2 \phi}{4}\right) \left[\left(\frac{\mu}{\sqrt{1 + 3 \cos^2 \phi}} - \frac{v\sqrt{3} \cos \phi}{\sqrt{1 + 3 \cos^2 \phi}} \right)^2 \delta\alpha_{\parallel} + \left(\frac{\mu\sqrt{3} \cos \phi}{\sqrt{1 + 3 \cos^2 \phi}} + \frac{v}{\sqrt{1 + 3 \cos^2 \phi}} \right)^2 \delta\alpha_{\perp} \right] + K \frac{\sin^2 \phi}{4} \delta\alpha_{\perp}, \quad (\text{B14})$$

$$\phi^1 = \arctan \left(\sin \phi \left(1 + \delta\alpha_{\perp} + \delta k_1 - \frac{2}{3} (\delta k_1 + \delta k_2 + \delta k_3) \right) \right). \quad (\text{B15})$$

We verified that when the results derived in Appendix A are combined with equations (16)–(18), the numerical results are identical to the outcome of the formulas derived in this section.

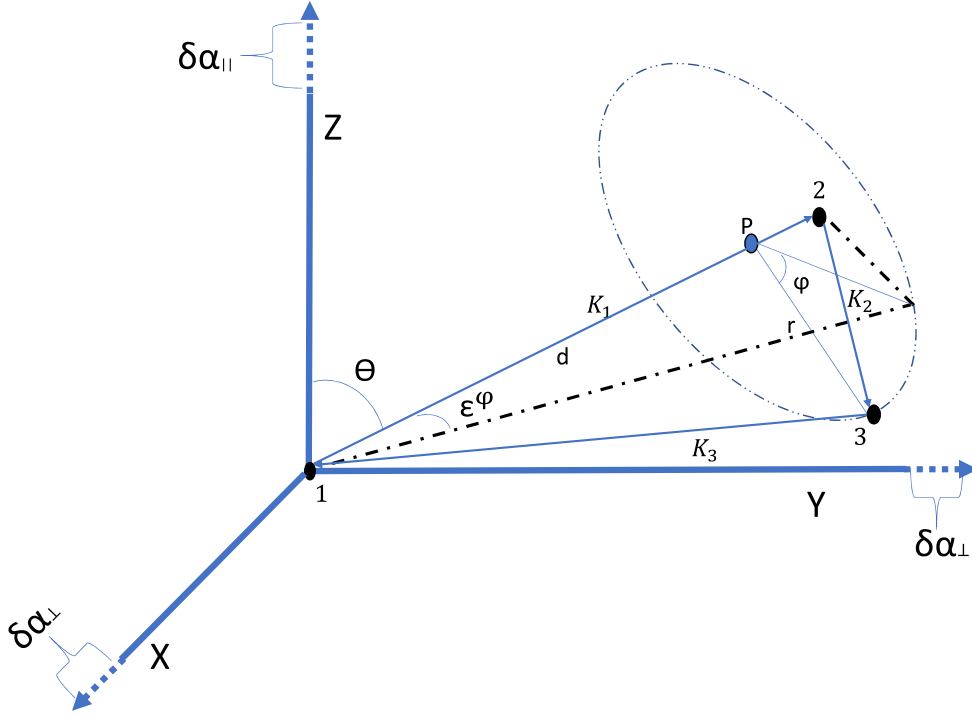


Figure B1. The same figure as in Fig. 1 with additional notations. Additional parameters that are defined are d (distance between point 1 and P), r (the radius of the circle around which point 2 can rotate with angle ϕ , giving us all possible spatial configurations of the triangle), and angle ξ^ϕ .

APPENDIX C: COMPUTING MODEL POWER SPECTRUM AND BISPECTRUM

We use linear perturbation theory to compute the model power spectrum and bispectrum for our validation tests presented in Figs 2 and 3 (Scoccimarro 2000; Gagrani & Samushia 2017).

We first compute the linear power spectrum P_{lin} using CAMB¹ software (Lewis & Bridle 2002). The galaxy power spectrum is then computed as

$$P(k) = (b_1 + f\mu^2) P_{\text{lin}}(k), \quad (\text{C1})$$

where b_1 and f are free parameters. We compute the bispectrum using

$$B(k_1, k_2, k_3) = 2Z_1(\mu_1)Z_1(\mu_2)Z_2(\mathbf{k}_1, \mathbf{k}_2)P_{\text{lin}}(k_1)P_{\text{lin}}(k_2) + \text{cyclic terms}, \quad (\text{C2})$$

where

$$Z_1(\mu) = (b_1 + f\mu^2), \quad (\text{C3})$$

$$Z_2(\mathbf{k}_1, \mathbf{k}_2) = \left\{ \frac{b_2}{2} + b_1 F_2(\mathbf{k}_1, \mathbf{k}_2) + f\mu_3^2 G_2(\mathbf{k}_1, \mathbf{k}_2) - \frac{f\mu_3 k_3}{2} \left[\frac{\mu_1}{k_1} (b_1 + f\mu_2^2) + \frac{\mu_2}{k_2} (b_1 + f\mu_1^2) \right] \right\}, \quad (\text{C4})$$

$$F_2(k_1, k_2) = \frac{5}{7} + \frac{\mathbf{k}_1 \cdot \mathbf{k}_2}{2k_1 k_2} \left(\frac{k_1}{k_2} + \frac{k_2}{k_1} \right) + \frac{2}{7} \left(\frac{\mathbf{k}_1 \cdot \mathbf{k}_2}{2k_1 k_2} \right)^2, \quad (\text{C5})$$

$$G_2(k_1, k_2) = \frac{3}{7} + \frac{\mathbf{k}_1 \cdot \mathbf{k}_2}{2k_1 k_2} \left(\frac{k_1}{k_2} + \frac{k_2}{k_1} \right) + \frac{4}{7} \left(\frac{\mathbf{k}_1 \cdot \mathbf{k}_2}{2k_1 k_2} \right)^2. \quad (\text{C6})$$

Cyclic terms are computed by permuting the indices (replacing 1 and 2 by 2 and 3, and then by 3 and 1 in the above equations).

This paper has been typeset from a $\text{\TeX}/\text{\LaTeX}$ file prepared by the author.

¹https://lambda.gsfc.nasa.gov/toolbox/camb_online.html

Investigating the Galaxy Cluster A3407 and the Surrounding Large-Scale Structure using eROSITA Data

Adhishree Lahiri¹, Thomas Reiprich¹, Florian Pacaud¹, and Angie Veronica¹

¹*University of Bonn*

The galaxy cluster system A3407-08 was recently observed by the eROSITA observatory. Aside from the two galaxy clusters which are very close to each other, this system consists of a number of other sources near these two clusters, which presents the system as an intriguing candidate for investigation. In this work, extensive surface brightness and spectral analysis of the cluster A3407 was done, along with investigations into the nature of the surrounding sources as well as any possible interactions with said sources. The cumulative data of all four eROSITA all-sky surveys was used in this work to examine the region around the cluster A3407. The PIB subtraction, exposure correction, galactic absorption correction and imaging enhancements were applied on the raw data. The imaging analysis reveals that the cluster A3407 is surrounded by the cluster A3408 to the east, a galaxy group to the north, and the cluster AS0601 and a galaxy group to the south-west. From surface brightness analysis of A3407 it can be seen that the cluster has higher emissions in the north and east regions, possibly due to the galaxy group and A3408, respectively. The surface brightness analysis can also be used to investigate the emission in the region between the two clusters for the detection of emission from a potential filament. The spectral analysis of the cluster A3407 was done to obtain the temperature, abundance and normalization profiles for A3407. This was also used to obtain the temperature and subsequently calculate the mass and radius of cluster A3407 and some of the surrounding sources. These values were also compared with the values obtained in previous works. The X-ray data used in this work was also compared to the Planck 2018 y-maps and the Sydney University Molonglo Sky Survey (SUMSS) radio data.

Emulator for three-point correlation function

K. Nagainis¹, M. Guidi¹, and M. Moresco^{1,2}

1 Dipartimento di Fisica e Astronomia "Augusto Righi" - Alma Mater Studiorum Università di Bologna, via Piero Gobetti 93/2, 40129 Bologna, Italy

2 INAF-Osservatorio di Astrofisica e Scienza dello Spazio di Bologna, Via Piero Gobetti 93/3, 40129 Bologna, Italy

Analysing the large-scale structure of the universe provides a wealth of information about the cosmological parameters. Among the methods employed, the three-point correlation function (3PCF) stands out for its ability to extract rich statistical information on galaxy clustering, offering an excess of information and constraints compared to the widely studied two-point correlation function (2PCF). Not only is it an independent method of acquiring the cosmological parameters, but it can also probe the non-Gaussianity of the primordial density fluctuations and break the degeneracy between the galaxy bias and the clustering at a given scale.

One of the bottlenecks in using the 3PCF for cosmological analyses resides in the fact that the models that have been currently developed are extremely computationally expensive, making it very difficult to properly explore the posterior distribution also with a MCMC approach. Therefore, with the upcoming galaxy surveys of tens of millions of objects (such as Euclid), finding a faster method to estimate 3PCF is pivotal. To solve the problem, we constructed an emulator for the 3PCF models which allows us to significantly speed up the computations. Likewise, the use of an emulator significantly accelerates likelihood analysis, a crucial aspect given the potential complexity of estimating up to 20 cosmological parameters. It is expected that this new method will be a complementary tool to analyse the data from upcoming surveys of Euclid, Large Synoptic Survey Telescope (LSST) and Dark Energy Spectroscopic Instrument.

Noeleen Naidoo,^{*} Sunil D. Maharaj,[†] and Keshlan S. Govinder[‡]
*Astrophysics Research Unit, School of Mathematics,
Statistics and Computer Science, University of KwaZulu–Natal,
Private Bag X54001, Durban 4000, South Africa*
(Dated: March 11, 2024)

We use Lie groups to analyse a system of partial differential equations that arise from the model of a spherically symmetric radiating star undergoing gravitational collapse in general relativity. When solving such differential equations in general relativity, the theory of Lie groups stands out as one of the few systematic methods available. Notably, there has been no systematic analysis of the system of partial differential equations comprising the boundary condition and equation of state. Exploring the boundary condition in the presence of heat flux represents a long-standing and fundamental research challenge. Santos [1] made significant progress by deriving a boundary condition for a spherically symmetric radiating star, excluding shear, thereby advancing research in relativistic star modelling. Subsequently, this work paved the way for the development of multiple models of radiating stars incorporating different matter fields, including those incorporating shear [2], the cosmological constant [3], and a composite matter boundary condition [4].

The boundary condition can be expressed as a partial differential equation that must be solved to complete the stellar model. However, the complete or general solution for any of the different analytic forms of the boundary condition remains unknown. In this study, we systematically analyse the boundary condition and equation of state within the context of this radiating star model [5]. Employing the geometric Lie group approach, we analyse the resulting system of partial differential equations. Our group analysis yields novel classes of exact solutions, including acceleration, expansion, and shear in the presence of the cosmological constant. Moreover, our solutions encompass known exact solutions as special cases, including the Euclidean star model and the relativistic counterpart of the Newtonian star. The range of equation of state parameters allows for the interpretation of the solution as barotropic matter stars or dark energy stars. A specific case demonstrates the physical validity of the model, with the energy conditions being satisfied.

Lie symmetries frequently arise in differential equations in general relativity. As demonstrated in this study, they offer a valuable tool for gaining systematic geometric insights into these systems of differential equations.

-
- [1] N.O. Santos, *Mon. Not. R. Astron. Soc.* **216**, 403 (1985).
 - [2] E.N. Glass, *Gen. Relativ. Gravit.* **21**, 733 (1989).
 - [3] A.B. Mahomed, S.D. Maharaj, R. Narain, *Eur. Phys. J. Plus* **134**, 545 (2019).
 - [4] S.D. Maharaj, B.P. Brassel, *Eur. Phys. J. C* **81**, 783 (2021).
 - [5] N. Naidoo, S.D. Maharaj and K.S. Govinder, *Ann. Phys.* **452**, 169288 (2023).

^{*}Noeleen1.naidoo@gmail.com

[†]maharaj@ukzn.ac.za

[‡]govinder@ukzn.ac.za

Monge-Ampère Gravity at Cosmological Scales

MH. Namdar¹

¹Department of Physics, Shahid Beheshti University, Tehran, Iran

Monge-Ampère gravitation is a recent mathematical theory aiming at generalizing classical Newtonian gravitation, by replacing Poisson equation with its fully non-linear counterpart, the Monge-Ampère equation. We show in details how the Poisson equation can be obtained from the Monge-Ampère equation in the weak-field limit, and formulate the Monge-Ampère equation for symmetric systems. We demonstrate that the Monge-Ampère equation is invariant under translation and rotation and as such can form a viable physical theory. We then solve the equation analytically for density profiles commonly-used to model galaxies in the Universe: the punctual mass. Throughout we compare our results with the solutions of Poisson equation and show how Monge-Ampère equation reduces to the Poisson equation, in all these cases.

Knowlegments:

I would like to extend my gratitude to my Supervisors, **Dr. Nima Khosravi** and **Dr. Farnik Nikakhtar** for all their support. I am also very thankful to **Prof. Roya Mohayaee** for her comprehensive assistance. Additionally, I would like to thank ICTP for providing me with this significant opportunity.

References

- [1] Albert Bonnefous, Yann Brenier, Roya Mohayaee, *Monge-Ampère gravity, optimal transport theory and their link to the Galileons*, 2024. arXiv:2405.15035 [gr-qc].
- [2] Kaare Brandt Petersen, Michael Syskind Pedersen, and others, *The matrix cookbook*, Technical University of Denmark, 2008.
- [3] Bruno Lévy, Yann Brenier, Roya Mohayaee, *Monge Ampère gravity: from the large deviation principle to cosmological simulations through optimal transport*, 2024. arXiv:2404.07697 [astro-ph.CO].

Self-Similarity of Halo Shapes for Power-law EdS Universe

Ayan Nanda^{1,2}, Nishikanta Khandai^{1,2}

¹*School of Physical Sciences, National Institute of Science Education and Research, Jatni
752050, India*

²*Homi Bhabha National Institute, Training School Complex, Anushaktinagar, Mumbai
400094, India*

We investigate the shapes of dark matter haloes in a cosmological N-body simulation utilizing the Gadget4[1] code within an Einstein-de Sitter (EdS) universe with power-law power spectrum.

The distribution of axis ratios for halo shapes shows a self-similar behavior when mass is appropriately scaled up. We extend our analysis to the computation of the velocity ellipsoid tensor, showing self-similarity in the asphericity of the velocity ellipsoid with proper mass scaling. We also find the mean axis ratios of the halo shapes and the velocity ellipsoid tensor as a function of scaled mass ($\frac{M}{M_{nl}}$) follow a single line independent of spectral index.

Our findings in the self-similar behavior of the distribution of axis ratios and the universal trend in the mean axis ratios across spectral indices ($-0.5, -1.0, -1.5$) suggests an analytical model which may give some intuition of this kind of trend.

References

- [1] Volker Springel, Rüdiger Pakmor, Oliver Zier, and Martin Reinecke. Simulating cosmic structure formation with the GADGET-4 code. *Monthly Notices of the Royal Astronomical Society*, 506(2):2871–2949, September 2021. doi: 10.1093/mnras/stab1855.

Examining cosmic (an)isotropy using velocity dispersion scaling relations of galaxy clusters

Aditya Pandya¹, Konstantinos Migkas², Thomas. H. Reiprich¹, Adam Stanford³, Florian Pacaud¹, Gerrit Schellenberger⁴, Lorenzo Lovisari^{4,5}, Miriam E. Ramos-Ceja⁶, Nhan T. Nguyen-Dang⁷, and Sangwoo. Park^{8,9}

¹*Argelander-Institut für Astronomie (AlfA), Universität Bonn, Auf dem Hügel 71, 53121 Bonn, Germany*

²*Leiden Observatory, Leiden University, PO Box 9513, NL-2300 RA Leiden, The Netherlands*

³*University of California, Davis, CA 95616, USA*

⁴*Center for Astrophysics | Harvard & Smithsonian, 60 Garden St., Cambridge, MA 02138, USA*

⁵*INAF, Istituto di Astrofisica Spaziale e Fisica Cosmica di Milano, via A. Corti 12, 20133 Milano, Italy*

⁶*Max Planck Institute for Extraterrestrial Physics, Giessenbachstrasse 1, 85748 Garching, Germany*

⁷*Institute for Astronomy and Astrophysics of Tübingen (IAAT), Germany.*

⁸*Korea Astronomy and Space Science Institute, Daejeon 34055, Republic of Korea*

⁹*University of Science and Technology, Daejeon 34113, Republic of Korea*

In standard cosmology, the late Universe is assumed to be statistically homogeneous and isotropic. This assumption suggests that the expansion rate of the Universe, as measured by the Hubble parameter, should be the same in all directions. Galaxy cluster scaling relations provide an excellent tool to test this hypothesis by pairing a cosmology-dependent quantity with a cosmology-independent quantity.

This work uses the velocity dispersion of galaxy clusters (σ_v) as the cosmology-independent quantity since its measurement does not involve cosmological assumptions. This quantity is paired with the cluster's X-ray luminosity (L_X) and the total integrated Compton parameter (Y_{SZ}), which are both dependent on cosmological parameters such as the Hubble constant (H_0). We constrain the apparent H_0 variations using the $L_X - \sigma_v$ and $Y_{SZ} - \sigma_v$ in different sky patches across the full extra-galactic sky. We utilise Monte Carlo simulations of isotropic cluster samples to quantify the statistical significance of any observed anisotropies.

From the joint analysis of the $L_X - \sigma_v$ and $Y_{SZ} - \sigma_v$ relations, the maximum variation of H_0 was found in the direction of $(l, b) = (280^\circ \pm 40^\circ, -35^\circ \pm 40^\circ)$ with a statistical significance of $\sim 3.72\sigma$.

Gravitational slip parameter and gravitational waves in Einstein–Cartan theory

Maryam Ranjbar¹, Siamak Akhshabi¹, and Mohsen Shadmehri¹

¹ *Department of Physics, Faculty of Sciences, Golestan University, Gorgan, Iran*

General Relativity (GR) has successfully predicted numerous phenomena. However, several mysteries persist in the realm of physics. One potential reason for these uncertainties is that GR, in the context of quantum mechanics, is fundamentally a classical theory. It is primarily tailored for the analysis of macroscopic phenomena. To address this limitation and extend the scope of GR to microphysical processes, various modified gravity theories have been proposed. Notably among them are those that factor in the torsion of spacetime, which is described as the non-symmetric part of the affine connection. The simplest of such theories is Einstein-Cartan theory (ECT), where torsion is coupled to the spin angular momentum of the matter fields which acts as a source for gravitational interactions.

Within the framework of ECT, the presence of torsion can introduce notable changes in the generation and propagation of gravitational waves [1]. Given that, investigating the behavior of GW through the ECT not only allows us to test the validity of this model, but also has the potential to reveal novel understandings regarding the nature of gravity.

Considering the perturbations level, there is an approach that is fully model-independent. This measures properties like the anisotropic stress without making any assumptions about the nature of the dark energy. The existence of anisotropic stress results in the appearance of gravitational slip i.e. the slip parameter η defined as the ratio between two gravitational potentials in a perturbed Friedmann-Robertson-Walker (FRW) universe being different from unity. Given that the contribution of neutrinos' free streaming to the anisotropic pressure in the late stages of the universe becomes negligible in the presence of perfect fluid matter, the only source of anisotropic stress could be a modification of gravity. In other words, the existence of anisotropic stress leads to a difference in values between the two scalar gravitational potentials that appear in the linear perturbation equations of motion and can be described as the gravitational slip parameter $\eta \equiv \frac{\Phi}{\Psi} \neq 1$ [2 – 6]. The advantages of the gravitational slip parameter are that it can be constructed based on model-independent observable quantities, and it is related to gravitational waves.

Motivated by the above mentioned discussions, We study the evolution of scalar and tensor cosmological perturbations in the framework of the Einstein-Cartan theory of gravity. The value of the gravitational slip parameter which is defined as the ratio of the two scalar potentials in the Newtonian gauge, can be used to determine whether or not the gravity is modified. We calculate the value of slip parameter in the Einstein-Cartan cosmology and show that it falls within the observed range. We also discuss the evolution of the cosmic gravitational waves as another measure of the modification of gravity.

- [1] E. Elizalde, and others, *Physics of the Dark Universe* **40**, 101197 (2023).
- [2] A. M. Pinho, S. Casas, and L. Amendola, *JCAP* **11**, 027 (2018).
- [3] L. Amendola, M. Kunz, M. Motta, I. D. Saltas, and I. Sawicki, *Phys. Rev. D* **87**, 023501 (2013).
- [4] M. Motta, I. Sawicki, I. D. Saltas, L. Amendola, and M. Kunz, *Phys. Rev. D* **88**, 124035 (2013).
- [5] I. D. Saltas, I. Sawicki, L. Amendola, and M. Kunz, *Phys. Rev. D* **113**, 191101 (2014).
- [6] L. Amendola, S. Fogli, A. Guarnizo, M. Kunz, and A. Vollmer, *Phys. Rev. D* **89**, 063538 (2014).

Modelling the stellar neutrino spectrum

Daniel Rodrigues¹

¹ *Department of Physics and Astronomy, University of British Columbia, Vancouver, Canada*

This study presents a simple model to the energy spectrum of stellar neutrinos as a step towards a more complete theoretical understanding of the extragalactic neutrino background. We use the well-established solar neutrino spectrum from the BS05[1] SSM (Standard Solar Model) and redshift surveys to estimate the neutrino flux coming from stars beyond our galaxy.

[1] Bahcall, J. N., Serenelli, A. M., & Basu, S. 2005, ApJ, 621, L85

Covariance matrices for 3-point correlation functions in photometric galaxy surveys.

Sofía Samario¹, Alejandro Avilés¹, and Juan Carlos Hidalgo¹

¹*Instituto de Ciencias Físicas, Universidad Nacional Autónoma de México, México*

The matter distribution in the Universe and its evolution give us important information about its components, such as the amount of baryonic matter, dark matter and dark energy, as well as the interactions between them. In order to know those characteristics, we study the statistical distribution of the objects in our Universe. The theory of Inflation predicts that the primordial density of fields is Gaussian, and therefore, we can describe them completely with the two-point correlation functions (2PCF). However, the Universe evolves, and the matter densities grow up by gravitational collapse and they enter in the non-linear regime. When this happens, the three-point correlation function (3PCF) is different from zero and gives us additional information from the 2PCF. In order to obtain this information we have to compare the observations with the theoretical models, hence we need the 3PCF and additionally a covariance matrix. Both of them allow us to have a good estimation of cosmological parameters. On the other hand, nowadays the galaxy surveys do not have enough number of objects and neither the accuracy needed, as a result of this we have obtained limited results on higher-order statistics with spectroscopic and photometric surveys. But this situation will change, thanks to catalogs such as LSST (Legacy Survey of Space and Time) from the Vera Rubin Observatory [1]. In this work we compute the covariance matrix of the 3PCF in a plane wave expansion for the convergence of weak lensing in photometric surveys of galaxies. This work will be published in a forthcoming paper [2].

[1] The LSST Dark Energy Science Collaboration (DESC) Science Requirements Document
LSST Dark Energy Science Collaboration • Rachel Mandelbaum(Carnegie Mellon U.) et al. e-Print:
1809.01669

[2] Samario Sofía, A. Avilés, J. C. Hidalgo (In preparation).

Abstract template for ICTP Summer School on Cosmology

M. Sekatchev¹, A. Zhitnitsky¹, and L. Van Waerbeke¹

¹*University of British Columbia, Department of Physics and Astronomy*

Telescope observations of background radiation in the Milky Way point to an anomalous excess in ultraviolet [4], radio [1], and x-ray [2] signals. The unconventional Axion Quark Nugget (AQN) dark matter model may provide an interpretation for this as-yet-unexplained excess. The model proposes that dark matter is dominated by macroscopic composite objects of nuclear density, in the form of matter and antimatter nuggets (see [5] for a recent brief review). Baryonic matter from ionized gas in the Warm Hot Intergalactic Medium (WHIM) surrounding the Milky Way may collide with antimatter AQNs and annihilate, resulting in an emission of a broad spectrum of electromagnetic radiation similar in form to Bremsstrahlung. The resulting spectrum was estimated to match the excesses in radio [3], UV [6], and x-ray [2] signals in the galaxy. The aim of this project is to compare the AQN annihilation radio emissions with the observed radio haze from WMAP. This is done by computing the signal from AQN annihilations within a cosmological hydrodynamic simulation of a Milky Way-like galaxy, and using a Markov chain Monte Carlo method to produce constraints on the AQN mass range and the dark matter density distribution. Understanding the source(s) of this excess radiation in our galaxy may bring us a step closer to revealing the nature of dark matter.

References

- [1] Douglas P. Finkbeiner. Microwave interstellar medium emission observed by the wilkinson microwave anisotropy probe. *The Astrophysical Journal*, 614:186–193, 10 2004.
- [2] Michael McNeil Forbes and Ariel R. Zhitnitsky. Diffuse x-rays: Directly observing dark matter? *JCAP*, 0801:023, 2008.
- [3] Michael McNeil Forbes and Ariel R. Zhitnitsky. WMAP Haze: Directly Observing Dark Matter? *Phys. Rev.*, D78:083505, 2008.
- [4] Richard Conn Henry, Jayant Murthy, James Overduin, and Joshua Tyler. The mystery of the cosmic diffuse ultraviolet background radiation. *The Astrophysical Journal*, 798(1):14, dec 2014.
- [5] Ariel Zhitnitsky. Axion quark nuggets. dark matter and matter–antimatter asymmetry: Theory, observations and future experiments. *Modern Physics Letters A*, 36(18):2130017, may 2021.
- [6] Ariel Zhitnitsky. The mysterious diffuse uv radiation and axion quark nugget dark matter model. *Physics Letters B*, 828:137015, 2022.

Self similar collapse of a tri-axial halo with baryons in an EdS universe

Siddhant sen¹, Susmita Adhikari^{1,2}

¹*(Presenting author underlined) Affiliation 1*

²*Affiliation 2*

We investigate the process of halo formation originating from initially scale-free perturbations, wherein gravitational collapse exhibits self-similarity. Previous studies by Fillmore and Goldreich (1984) and Bertschinger (1985) have successfully addressed the one-dimensional (spherically symmetric) scenario. Expanding upon their work, we extend these findings to three-dimensional, triaxial self-similar equations along with the inclusion of the baryons. Through semi-analytical numerical simulations, we solve these equations and conduct a detailed analysis of the resulting similarity solutions, with a specific focus on elucidating the relationship between the shock and splashback radius of the collapsed halos. We will eventually compare our halos to those arising from initial perturbations in realistic N-Body and hydrodynamical simulations.

References

- [1] Bertschinger, E. 1985, ApJS, 58, 39.
- [2] Fillmore, J. A., Goldreich, P. 1984, ApJ, 281, 1
- [3] arXiv:1010.3723 [astro-ph.CO]

Constraining Horndeski Gravity on Cosmological Scales

Neel Shah¹, Johannes Noller^{1,2,3}, Kazuya Koyama¹

¹*(Presenting author underlined) Institute of Cosmology & Gravitation, University of Portsmouth, Portsmouth, PO1 3FX, U.K.*

²*Department of Physics & Astronomy, University College London, London, WC1E 6BT, U.K.*

³*DAMTP, University of Cambridge, Wilberforce Road, Cambridge, CB3 0WA, U.K.*

Horndeski gravity is the most general class of models of gravity that incorporates a single extra scalar degree of freedom in the gravitational sector and leads to equations of motion with at most two spacetime derivatives. In the context of cosmology, we can encode the entire variety of models in this class into five arbitrary functions of time, each having a unique phenomenological effect beyond Λ CDM cosmology. This combination of simplicity in the theoretical expressions and richness of phenomenological predictions makes cosmology a powerful probe of Horndeski gravity. I will talk about the impact that various theoretically and observationally motivated priors and parametrizations have on the cosmological constraints on Horndeski gravity.

Exploring the correlations between galaxy properties and environment in the cosmic web using marked statistics

Unnikrishnan Sureshkumar^{1,2}

¹*(Presenting author underlined) Wits Centre for Astrophysics, University of the Witwatersrand, Johannesburg, South Africa*

²*Astronomical Observatory of the Jagiellonian University, Krakow, Poland*

Various galaxy properties such as luminosity, stellar mass, star formation rate and so on are known to be significantly correlated with the local environment of the galaxies in the cosmic web. These correlations arise from the environmental dependence of their dark matter halo properties. Studies on such environmental correlations are crucial for better understanding of galaxy evolution. These studies are generally done using local density measurements defined at a particular separation scale around the galaxies. However, it is essential to study environmental correlations on a wide range of scales. This approach helps in the investigation of environmental effects that are prevalent at different scales as well as minimising the impact of the chosen scale for density estimation. In this poster, I will show how marked correlation functions are efficient in tracing the environmental correlations of various galaxy properties simultaneously as a function of the separation scale. I will present results from our studies that investigated how luminosities in optical to mid-IR bands, stellar mass, and star formation rate are correlated with the local environment [1, 2]. Additionally, I will show how the marked correlation function is advantageous over traditional two-point correlation functions to explore the environmental dependence of galaxy mergers [3]. Our analysis utilises stellar-mass-selected volume-limited galaxy samples from the Galaxy And Mass Assembly (GAMA) survey.

[1] U. Sureshkumar, A. Durkalec, A. Pollo, et al., *A&A* **653**, A35 (2021).

[2] U. Sureshkumar, A. Durkalec, A. Pollo, et al., *A&A* **669**, A27 (2023).

[3] U. Sureshkumar, A. Durkalec, A. Pollo, et al., *A&A* **686**, A40 (2024).

Testing Beyond- Λ CDM Cosmologies with Neural Networks

Linus Thummel^{1,2}, Benjamin Bose¹, and Alkistis Pourtsidou^{1,2}

¹ *Institute for Astronomy, University of Edinburgh, Royal Observatory, Blackford Hill, Edinburgh, EH9 3HJ, U.K.*

² *Higgs Centre for Theoretical Physics, University of Edinburgh, Edinburgh EH9 3FD, U.K.*

Forthcoming stage-IV cosmological surveys will perform measurements with unprecedented accuracies up to non-linear scales. We have developed a novel machine learning approach to detect beyond-standard-model physics in the data using a Bayesian Neural Network [1]. The purpose of this machine-learning based method is not the replacement of an MCMC analysis, but the development of a tool that can reduce the vast landscape of modified gravity and dark energy theories with high time efficiency.

We use non-linear dark matter power spectra to train the Bayesian Cosmological Network (BaCoN [2]) that can classify spectra into one of 5 classes: Λ CDM, $f(R)$, w CDM, Dvali-Gabadaze-Porrati (DGP) gravity and a ‘random’ class. The modelling includes baryonic effects and massive neutrinos to increase the accuracy on non-linear scales and enhance our ability to detect deviations from Λ CDM [3]. We further develop the treatment of theoretical errors in BaCoN to enable the trained network to generalise to other power spectrum modelling prescriptions. Our fiducial classifier, trained with the optimal theoretical error model, achieves a total classification accuracy of $\sim 95\%$. This greatly bolsters the promise of this method to glean the maximal amount of unbiased gravitational and cosmological information from forthcoming Stage-IV galaxy surveys.

[1] L. Thummel, B. Bose, A. Pourtsidou and L. Lombriser, arXiv preprint **2403.16949** (2024).

[2] M. Mancarella, J. Kennedy, B. Bose, and L. Lombriser, Phys. Rev. D **105**, 23531 (2022).

[3] B. Bose, B. S. Wright, M. Cataneo et al, MNRAS **508**, 2479 (2021).

Detectability of PBHs by Lensed GW events

Nooshin Torabi¹, Shant Baghram¹, and Sohrab Rahvar¹

¹*Department of Physics, Sharif University of Technology, P. O. Box 11155-9161, Tehran, Iran*

Massive objects in the universe cause deflection of the light rays on their path from the source to the observer; this phenomenon called Gravitational Lensing happens to gravitational waves similar to light rays. Gravitational waves produced by events such as the merger of binary black holes, binary neutron stars, or neutron star-black hole binaries are powerful enough to be detected by the observational power of modern observatories.

In the case of Strong lensing, creating two or even multiple images with different magnifications of an event is possible. The images reach the observer with a time delay. If a galaxy acts as a gravitational lens, the time delay could be on the order of minutes to months, and if a cluster lies in the path of the waves, it could be on the order of years. Cross section of Strong lensing depends on the lens model and the corresponding Einstein radius.

Gravitational Lensing can be studied in two regimes: geometrical optics and wave optics. When the wavelength of the waves is smaller than the Schwarzschild radius of the lens, geometrical optics is sufficient to study the lensed signal, and when the wavelength is comparable to or larger than the Schwarzschild radius of the lens, wave effects become significant causing beating patterns in the signal.

Strong lensing statistics could provide us information about the expected number of lensed events that reach an observer, and the time delay distribution, which helps us determine if we could detect separate images with a given detector and observation duration and also magnification distribution of different images of the same event which would be useful in determining the detectability of the signal by a given threshold and sensitivity.

To determine the expected number of lensed events we need to calculate the merger rate of black holes, the probability of lensing which is capsulated in optical depth, and the detectors' characteristics. Different lens models could lead to different optical depths and thus change the number of lensed events. Many papers have worked on different scenarios and calculated the number of lensed events for different telescopes.

The existence of Primordial black holes, which has been a subject of debate in the field, could affect the lensing rate due to acting like a point mass lens. Furthermore, because of the range of frequencies that we detect gravitational waves, wave optics can play an important role in lensing. In a previous work [1], the possibility of detecting GW lensing by considering only PBHs has been studied.

In this study, we aim to investigate how considering primordial black holes as a fraction of dark matter in the universe would change the expected number of lensed GW events and if lensing by primordial black holes is divisible from the effect of dark matter halos and also observable by current and future detectors considering the role of wave optics.

[1] E. Khalouei, H. Ghodsi, S. Rahvar, and J. Abedi, *Phys. Rev. D* **103**, 084001 (2021).

Effects of Dark Matter Particles in Compact Objects and Observational Constraints

Bruna V. Simão¹, Tiago J. N. Silva¹, and André S. Schneider¹

¹*Universidade Federal de Santa Catarina*

In addition to black holes, neutron stars (NSs) are known for being astrophysical objects with some of the strongest gravitational fields. This extreme feature makes them a powerful environment to probe dark matter particles (DM), whose interactions with the baryonic sector are given essentially through gravity. As it has been studied over the literature, compact objects such as neutron stars are capable of “capturing” dark matter and are natural laboratories for this sector [1]. An example is when dark matter is gravitationally attracted and accelerated to semi-relativistic velocities. The scattering particles on the surface are able to transfer kinetic energy to the star, increasing its temperature to compelling levels for observation [2, 3]. On the other hand, depending on the class the dark particles involved in this processes, the trapped matter can accumulate excessively in a massive core and cause the star to collapse into a black hole [4, 5]. Since dark matter can affect the properties and dynamic mechanisms of neutron stars and other compact objects, the observation of gravitational waves from collaborations such as LIGO-Virgo-KAGRA can potentially constrain different models of the dark sector of matter. Additionally, it is possible to probe them in other contexts, such as early universe phase transitions, which is a promising area of research in light of future low-frequency gravitational wave experiments as LISA [6, 7]. Therefore, investigating the nature of dark matter within stellar objects holds significant promise not only in particle physics, but also in astrophysics and cosmology. This work, which comprehends the first stage of a PhD project, provides the reader with a literature overview on this topic.

- [1] C. Kouvaris, P. Tinyakov, *Phys. Rev. D* **82**, 063531 (2010).
- [2] D. A. Camargo, F. S. Queiroz, R. Sturani, *JCAP* **09**, 051 (2019).
- [3] N. F. Bell, G. Busoni, S. Roble, *JCAP* **09**, 018 (2018).
- [4] R. Garani, Y. Genolini, T. Hambye, *JCAP* **05**, 035 (2019).
- [5] S. Gardner e M. Zaker, *Universe* **10**, 67 (2024).
- [6] J. Crowder, N. J. Cornish, *Phys. Rev. D* **72**, 083005 (2005).
- [7] G. Arcadi, G. C. Dorsch, J. P. Neto, F. S. Queiroz, Y.M. Oviedo-Torres, *Physics Letters B* **848**, 138382 (2024).

A line-of-sight CMB integrator for nearly-isotropic Bianchi models

João Gabriel Vicente¹, Thiago Pereira¹, and Cyril Pitrou²

¹ *Universidade Estadual de Londrina*

² *Institut d'astrophysique de Paris*

Bianchi models are a class of spatially homogeneous and anisotropic cosmologies. They are the simplest generalization of a FLRW Universe, and, in fact, some of them have a homogeneous and isotropic limit. As a consequence, the “almost FLRW” Bianchi models can be described as linear perturbations over a homogeneous and isotropic background. It is thus possible to systematically study these models in the context of standard perturbation theory [1] and to match each to a specific perturbation mode [2].

This methodology provides a way to understand how these special Bianchi models influence the large-angle anisotropies in the Cosmic Microwave Background: it is sufficient to write the Boltzmann hierarchy and solve it for the particular Fourier mode in which the Bianchi model corresponds to a large FLRW perturbation. This can be implemented by solving the hierarchy for small multipoles and then computing the line-of-sight integration in order to obtain higher ones.

We develop two softwares, Anilos (Anisotropic line-of-sight integrator) and Aniclass, that compute the line-of-sight integration of perturbations in nearly-isotropic Bianchi Universes. Anilos is an ease-to-modify code written in Python and Aniclass is a modification of CLASS that is optimal for statistical analysis. These implementations provide a fast method to compute the deterministic anisotropic patterns in the CMB in Bianchi VII_h , VII_0 , V, and IX cosmologies. Tensor and non-decaying vector perturbations are currently implemented. The latter is possible by the choice of specific initial conditions, and Anilos allows for simple modifications so that new initial conditions can be implemented and studied together with Bianchi cosmologies.

Anilos and Aniclass are targeted to CMB applications. However, given the simplicity of line-of-sight methods, it can be modified to encompass different cosmological observables, such as weak-lensing and redshift drifts. Such functionalities shall be implemented in future versions of Anilos.

[1] Pontzen, A., Challinor, A., *Classical and Quantum Gravity* **28**, 185007 (2011).

[2] Pereira, T., Pitrou, C., *Physical Review D* **100**, 123534 (2019).

Cosmological Field-Level Inference using Fast Differentiable Integrators

L. Winkler¹, F. List^{1,2}, and O. Hahn^{1,2}

¹*Department of Astrophysics, University of Vienna, Türkenschanzstraße 17, 1180 Vienna, Austria*

²*Department of Mathematics, University of Vienna, Oskar-Morgenstern-Platz 1, 1090 Vienna, Austria*

One of the most fundamental questions in cosmology is how structure formed in our universe from primordial perturbations to the objects we can observe today. The current standard model Λ CDM is mostly consistent with this, but next generation instruments like JWST, Euclid, LSST and DESI will be able to test its predictions with unprecedented accuracy. The primary tool to compare the influence of different cosmological models and parameters on structure formation are large-scale N-Body simulations. Recently fully differentiable simulations have enabled inferring the properties of the universe more efficiently. Combining this with better time integration methods that allow significantly faster simulations without sacrificing accuracy and field-level Bayesian inference, it is now possible to reconstruct the properties of our universe more accurately than ever before.

Boundary Correlators with Strongly-Coupled Exchange

Guilherme L. Pimentel¹ and Chen Yang¹

¹*Scuola Normale Superiore and INFN, Pisa*

It is a natural start-point for us to study the strongly-coupled correlators from the conformal exchange, since it has more symmetry constraints. In this talk, I will talk about four-point cosmological correlators in de Sitter with a strongly-coupled conformal exchange, which was first discussed in [1], and now we have more specific results for the four-point single-exchange case, using the cosmological bootstrap and Differential Equations techniques developed in [3] and [2]. I will also discuss a possible scaling flow which is similar to the kinematic flow found in [4]. If time permits, I will further discuss the behaviors of strongly-coupled correlators in de Sitter with a massive deformation to the conformal exchange case, using AdS/CFT techniques.

- [1] D. Green, M. Lewandowski, L. Senatore, E. Silverstein and M. Zaldarriaga, JHEP **10** (2013), 171 doi:10.1007/JHEP10(2013)171 [arXiv:1301.2630 [hep-th]].
- [2] N. Arkani-Hamed, D. Baumann, A. Hillman, A. Joyce, H. Lee and G. L. Pimentel, [arXiv:2312.05303 [hep-th]].
- [3] N. Arkani-Hamed, D. Baumann, H. Lee and G. L. Pimentel, JHEP **04** (2020), 105 doi:10.1007/JHEP04(2020)105 [arXiv:1811.00024 [hep-th]].
- [4] N. Arkani-Hamed, D. Baumann, A. Hillman, A. Joyce, H. Lee and G. L. Pimentel, [arXiv:2312.05300 [hep-th]].

Multifield inflation with massive fields and its impacts on early universe cosmological observables.

Cristóbal Zenteno Gatica¹.

1 Instituto de Física Teórica UAM/CSIC C/Nicolás Cabrera 13-15 Universidad Autónoma de Madrid Cantoblanco, Madrid 28049, Spain.

In the context of inflation driven by multiples degrees of freedom, the effects of interactions between the adiabatic (or curvature) and the isocurvature modes of the perturbations have been studied in the last years. These interactions have a significant relevance because they can trigger enhancements in the curvature perturbation. An amplification in the primordial curvature perturbation could have an impact in various observables, for example, the generation of primordial black holes (PBH) or the stochastic gravitational-wave background (SGWB). Recently, the fields' interactions, which (in our work-frame) can be understood as non-trivial trajectories in the field space, have been studied for the non-canonical regime (where the parameter that describes the interaction is greater than one) for a massless and massive isocurvature field. In this poster, following [1,2], we review the theoretical methods to represent the fields solutions and discuss the generation of enhancements and signatures on the primordial power spectrum that could affect the PBH formation and the SGWB. In particular, we are focused on how these solutions can be generalized for various interaction models and how we can trace the features of a certain inflationary model into the observables.

[1] G. A. Palma, S. Sypsas, and C. Zenteno, “Seeding primordial black holes in multifield inflation,” *Phys. Rev. Lett.*, vol. 125, no. 12, p. 121301, 2020.

[2] J. Fumagalli, G. A. Palma, S. Renaux-Petel, S. Sypsas, L. T. Witkowski and C. Zenteno, Primordial gravitational waves from excited states, *JHEP* 03 (2022) 196.